This article has been accepted for publication in IEEE Access. This is the author's version which has not been fully edited and content may change prior to final publication. Citation information: DOI 10.1109/ACCESS.2025.3565226

IEEE Access
Multidisciplinary ⋮ Rapid Review ⋮ Open Access Journal

Date of publication xxxx 00, 0000, date of current version xxxx 00, 0000.

Digital Object Identifier 10.1109/ACCESS.2024.0429000

Adaptive Hybrid Tripping Microgrid Protection Strategy with Embedded Hardware Validation

PEDRO H. A. BARRA[1], RICARDO A. S. FERNANDES[2] (Senior Member, IEEE), and DENIS V. COURY[2]

[1]Faculty of Electrical Engineering, Federal University of Uberlândia, Uberlândia, Minas Gerais, Brazil. (e-mail: pedrobarra@ufu.br)
[2]Department of Electrical and Computer Engineering, São Carlos School of Engineering, University of São Paulo, São Carlos, São Paulo, Brazil. (e-mail: coury@sc.usp.br)

Corresponding author: Denis V. Coury (e-mail: coury@sc.usp.br).

This work was supported in part by the São Paulo Research Foundation (FAPESP) [Grant Number 2023/00182-3] and the Minas Gerais Research Foundation (FAPEMIG) [Grant Number APQ-02230-24]

ABSTRACT This paper proposes an adaptive hybrid-tripping-based protection strategy for microgrids (MGs) that enables a fast and reliable response to faults by leveraging phase voltage and current measurements from relay locations. The protection coordination problem was addressed by optimizing the relay settings for different MG operating scenarios, ensuring proper coordination between the primary and backup relays. Comprehensive performance evaluation using PSCAD simulations demonstrated that the proposed protection scheme operates with 50% of faults cleared within 41.5 ms, while 90% of cases are cleared within 530.8 ms across various fault conditions in both grid-connected and islanded operating conditions. The backup relays exhibited a minimum trip time of 230 ms and a median trip time of 299.6 ms, while the coordination time intervals remained within safe margins (50% of cases maintaining a margin of 246.7 ms), ensuring selectivity. Moreover, real-time hardware-in-the-loop (HIL) tests using TMSF28335 microcontrollers validated the scheme's practical applicability, showing a strong correlation between simulated and experimental results. The mean difference between the simulated and experimental trip times was 29 ms, with maximum deviations below 7.2% (64 ms) and a minimum deviation of 5 ms. The results confirm the effectiveness of the proposed strategy in reducing tripping times while maintaining coordination, making it a promising solution for both islanded and grid-connected MG operating modes.

INDEX TERMS Adaptive protection, hardware-in-the-loop, microgrid, microgrid protection, non-standard protection curve.

I. INTRODUCTION

MICROGRIDS (MGs) have attracted considerable attention from distribution utilities, industry, and researchers in recent years. This is because MGs are in tune with the 3D framework (decarbonization, digitization and decentralization), as these three interconnected trends are transforming various fields, particularly the energy sector [1]. In addition, MGs play a key role in transforming conventional grids into modern, smart grids, enhancing their reliability and resilience [2].

MGs can integrate distributed energy resources (DERs), including distributed generators (DGs), energy storage systems, and loads [3], [4]. MGs can be found in low and medium voltages, with different sizes, functionalities, and configurations [5]. Moreover, MGs can integrate advanced communication, control, instrumentation and automation infrastructure, enabling efficient and reliable management of loads and DERs [6]–[8]. Noteworthy is that MGs have some possible configurations considering grid-connected and islanded modes, depending on their size and characteristics. Thus, MGs are connected to the main grid in a grid-connected mode through a point of interconnection (POI). Nonetheless, considering MGs' capability of a seamless transition to an islanded mode, they operate even after undesired events in the main grid. In addition, it is crucial to note that the ability of MGs to perform black starts and operate in islanded mode significantly improves the resilience and reliability of distribution systems in addressing contingencies, emergencies, and blackouts.

To fully leverage the potential of MGs while ensuring their safe operation, several challenges should be addressed during their planning and operation. Among these challenges, the following can be mentioned: energy management; stability; control; cybersecurity; and protection. Thus, it is important to note that conventional protection schemes used

This work is licensed under a Creative Commons Attribution 4.0 License. For more information, see https://creativecommons.org/licenses/by/4.0/

This article has been accepted for publication in IEEE Access. This is the author's version which has not been fully edited and content may change prior to final publication. Citation information: DOI 10.1109/ACCESS.2025.3565226

in traditional distribution systems may not perform effectively when addressing the unique challenges and situations encountered in MGs [9]–[11]. In MGs, fault currents vary substantially depending on the configurations, i.e., islanded or grid-connected modes, and the feasible MG operating scenarios. DERs can also considerably affect fault currents, depending on their status and type. Inverter-based DGs supply low fault currents, in contrast to synchronous-based ones. Furthermore, changes in MG topology may affect fault currents, considering self-healing and other conditions. The aforementioned concerns demonstrate the need to propose novel solutions and strategies to safeguard MGs in both grid-connected and islanded operating modes, ensuring optimal speed, selectivity, sensitivity, and reliability [9], [11]. Thus, this paper proposes a novel adaptive protection strategy for MGs based on new hybrid tripping characteristics. The key innovation lies in the development of new adaptive hybrid protection curves, specifically designed to address the challenges of protecting microgrids in both grid-connected and islanded operating modes. The non-standard curves proposed use only local current and voltage signals measured at the relays' locations, which greatly simplifies the proposition and improves its applicability. The proposed strategy adapts effectively to varying fault current levels, providing a fast and reliable response in both scenarios. Furthermore, the flexibility of the new strategy was validated through PSCAD simulations and hardware-in-the-loop (HIL) testing with a real-time digital simulator (RTDS), demonstrating its robustness under different MG operating conditions. Therefore, the contributions of this paper can be summarized as the following:

- The strategy introduces new protection curves, proving to be effective for MG operational scenarios. These curves were designed taking into account the existing challenges in protecting MGs.
- The technique covers grid-connected and islanded modes, presenting adequate results and coordination. Therefore, it is unnecessary to use different protection methods for each operating mode.
- The methodology is adaptive and uses optimized protection settings depending on the MG scenario. Thus, protection responses tend to be faster for any configuration.
- The approach was embedded in hardware to be validated through HIL tests, showing a dependable response and practicability in terms of instrumentation for MGs. The reliable real-time operation of the proposition demonstrates its practical applicability.

The remainder of the paper is organized as follows. Section II discusses existing research on the topic. Section III presents the conceptual design of the proposed approach. Section IV provides the performance evaluation of the proposed protection strategy using simulation results. Section V shows the HIL validation of the proposal. Section VI discusses the results. Finally, Section VII draws the conclusions.

II. BACKGROUND REVIEW

Different strategies have been proposed in the literature to address the mentioned concerns. In [12], a waveform difference feature-based protection scheme was proposed, using the angle difference of the positive sequence of the fault current, as well as the mathematical morphology. It is important to highlight that restricting the method to the islanded operation mode significantly limits its applicability, especially in scenarios where grid-connected operation is essential. In addition, the lack of relay coordination can compromise the security and reliability of the protection system. Given that MG protection is the central focus of the study, not addressing these aspects represents a significant limitation of the proposed approach. Dual setting protection of MG was proposed in [13], where two time dial settings and a pickup current setting were adjusted for each relay, regardless of the MG's connection mode. Despite demonstrating promising performance, the study is constrained by the limited number of operating scenarios analyzed. Additionally, the performance of the approach on hardware was not assessed, which is crucial for practical validation. This omission reduces the credibility of the proposed scheme when applied in real-world MG environments. Reference [14] presented an adaptive current-angle-based approach. It used a phase selection method and created fault-type adaptive zones for MG protection. However, this work did not address the coordination issue, which is a critical factor in MG protection schemes. Furthermore, the hardware implementation of the approach was not investigated either, which limits the practical applicability of the method.

Adaptive protection using micro-phasor measurement units and overcurrent protection was presented in [15]. Thévenin impedance at the POI of the MG was used to re-optimize the relays' coordination. While this approach offers a promising method for adaptive protection, its main shortcoming is the requirement to allocate multiple micro-phasor measurement units throughout the MG. This requirement significantly increases the cost and complexity of the implementation, potentially limiting the practical adoption of the method. Furthermore, the authors of [16] proposed an integrated impedance angle-based MG protection scheme. The approach yielded adequate results, however, it was limited to fault detection. Another drawback is that it requires phasor measurement units in all MG buses, increasing cost and complexity. Approaches based on the injection of synthetic harmonic current patterns after fault inception can be found in [17]–[19]. Injection of harmonic patterns can be a way to easily detect MG faults. However, the main drawback of these approaches is the need to alter the DER controllers, which is not always straightforward from a practical point of view. Additionally, all of these methods were designed exclusively for an islanded operating mode, which required further research on their adaptation for grid-connected scenarios.

In [20], the voltage phase angle shift and the difference between the predicted and actual current samples were used to protect the MGs. This paper presented promising results with a low fault detection time. However, the study failed

This work is licensed under a Creative Commons Attribution 4.0 License. For more information, see https://creativecommons.org/licenses/by/4.0/

This article has been accepted for publication in IEEE Access. This is the author's version which has not been fully edited and content may change prior to final publication. Citation information: DOI 10.1109/ACCESS.2025.3565226

to address coordination methods concerning relay operation, limiting its broader application in complex MG systems. In [21], a topology-agnostic, scalable, and cost-aware protection scheme was proposed, including a stable automatic reconfiguration of healthy sections. The online operation of this approach highly depends on communication infrastructure, which introduces potential vulnerabilities in case of communication failures. Furthermore, no experimental validation was performed, limiting the practical verification of the proposed scheme. In [22], the selectivity problem was investigated when using overcurrent protection for MGs. The authors proposed using the overcurrent relays' definite-time characteristics when the MG operated in an islanded mode, whereas the conventional one worked for the grid-connected mode. This approach resulted in high tripping times for an islanded mode and lacked scalability regarding some scenarios.

An MG protection coordination strategy considering clustering and metaheuristic optimization was proposed in [23]. Although the study introduces an interesting approach by integrating unsupervised learning techniques, metaheuristic optimization, and non-standard protection curves to define setting groups, it falls short in demonstrating the practical applicability of the proposed method. The lack of experimental validation, as well as omitting fault types and resistance variations, raise concerns about its robustness and real-world feasibility application. Reference [24] proposed a novel protection design process aimed at improving MG resilience. Although the study effectively highlights the impact of protection strategies on the resilience of MGs, its applicability is limited, as the proposed approach is designed exclusively for islanded MGs, leaving its effectiveness unaddressed in grid-connected or transitioning modes.

Recent works have explored machine learning algorithms as tools for MG protection [25]–[28]. In [25], a deep learning-based protection scheme was proposed to identify faults in MGs, achieving a reported accuracy of 98.94%. However, critical aspects such as relay coordination, backup protection, and experimental validation were not addressed, raising concerns about the scheme's real-world applicability. Similarly, in [26], the authors introduced a multi-agent deep learning-based protection system, demonstrating an accuracy of 99.25% in detecting and isolating faulty phases. Although promising, the study lacks a comprehensive analysis of fault conditions, does not provide details on the neural network training process, and omits experimental validation, which undermines confidence in its practical deployment. Furthermore, the complexity of the proposed method may pose challenges for implementation in real-world MGs. These same limitations (restricted fault scenarios, absence of experimental verification, and practical deployment challenges) were also evident in [27], [28], highlighting a common gap in current machine learning-based approaches.

Some of the aforementioned papers have used standard protection curves, such as the traditional ones described in the IEEE Std. C37.112-2018 [29]. However, despite operating in most commercial relays of distribution systems, standard curves (even standard voltage-restrained overcurrent ones) may present some flaws when addressing MG challenges. To overcome these difficulties, the authors of [30]–[33] proposed new relay characteristics for MG protection. Despite offering improved performance, several gaps remain. Most of these studies lack hardware assessments, crucial for evaluating the applicability of proposed curves in real-world MG environments. Furthermore, adaptive strategies, which could enhance overall protection performance, were not explored in depth. Lastly, most studies applied the proposed curves in a limited number of MG operating scenarios, often disregarding the islanded or grid-connected modes, as well as coordination tasks.

Table 1 summarizes the main information of the revised papers, comparing them with the proposed adaptive protection strategy. This comparison covers two main aspects: (i) method considerations; and (ii) method evaluation and results. All of their characteristics are discussed next:

- **A1** – *Input signals* – indicate the input of the proposed protection schemes. Note that most consider both current and voltage signals;
- **A2** – *Coordination strategies* – indicate if a paper considers a coordination strategy among the relays. Some papers do not consider a coordination strategy, indicating a limitation of the proposed protection;
- **A3** – *Diversified optimization techniques* – indicate if the coordination optimization problem was analyzed (when applicable) with a variety of optimization techniques. Most papers do not consider different techniques, indicating a possibility for future research;
- **A4** – *Adaptive characteristics* – indicate if the method has an adaptive characteristic that increases the protection flexibility. A minor part of the revised papers has this advantage;
- **A5** – *Backup protection* – indicates if the proposed scheme considers backup protection for primary relays. If primary protection fails, the backup relays should operate. This characteristic is important for a dependable protection and was not considered in most methods;
- **A6** – *Non-standard protection curves*– indicate if the research proposed or considered any type of non-standard protection curve;
- **A7** – *Dynamic simulations* – indicate if the research considered/presented dynamic simulations. These simulations represent more realistic results;
- **A8** – *Sampling frequency* – shows the sampling frequency value, when informed in the paper. Few papers indicate this important information. Commercial values are desired here;
- **A9** – *Grid-connected mode* – indicates if the protection method works in a grid-connected operating mode;
- **A10** – *Islanded mode* – indicates if the protection method works in an islanded operating mode;
- **A11** – *Self-healing switching and contingencies* – indicate if self-healing actions are evaluated;

This work is licensed under a Creative Commons Attribution 4.0 License. For more information, see https://creativecommons.org/licenses/by/4.0/

This article has been accepted for publication in IEEE Access. This is the author's version which has not been fully edited and content may change prior to final publication. Citation information: DOI 10.1109/ACCESS.2025.3565226

TABLE 1. Comparison of the proposed method with the existing research

Reference	Method Considerations						Method Evaluation & Results						
	A1	A2	A3	A4	A5	A6	A7	A8	A9	A10	A11	A12	A13
[12]	θ_{I+}	✗	✗	✗	✗	✗	✗	5 kHz	✗	✓	✗	✗	✗
[13]	I	✓	✗	✗	✓	✗	✗	–	✓	✓	✗	✗	✗
[14]	$\theta_{I+}\&\theta_{V+}$	✗	✗	✓	✗	✗	✓	–	✓	✓	✗	✗	✗
[15]	$I\&V$	✓	✗	✓	✓	✗	✗	–	✓	✗	✗	✗	✗
[16]	$I\&V$	✗	✗	✗	✗	✗	✓	–	✓	✓	✗	✗	✗
[17]	$I\&V$	✗	✗	✗	✓	✗	✓	–	✗	✓	✓	✗	✗
[23]	I	✓	✓	✓	✗	✓	✗	–	✓	✓	✗	✗	✗
[24]	I	✓	✓	✓	✗	✓	✓	–	✗	✓	✗	✗	✓
[25]	$I\&V$	✗	✗	✗	✗	✗	✓	–	✓	✓	✗	✗	✗
[27]	$I\&V$	✗	✗	✓	✗	✗	✓	1 kHz	✓	✓	✗	✗	✗
[26]	I	✗	✗	✗	✗	✗	✗	3.84 kHz	✓	✓	✗	✗	✗
[28]	$I\&V$	✗	✗	✗	✗	✗	✗	–	✓	✓	✓	✗	✗
[30]	I	✓	✗	✗	✓	✓	✗	–	✓	✓	✗	✗	✗
[31]	I	✓	✗	✗	✓	✓	✗	–	✓	✓	✗	✗	✗
[32]	I	✓	✗	✗	✓	✓	✗	–	✓	✓	✗	✗	✗
[33]	$I\&V$	✓	✗	✗	✗	✓	✓	1.92 kHz	✓	✓	✗	✗	✗
Proposed method	$I\&V$	✓	✗	✓	✓	✓	✓	1.92 kHz	✓	✓	✓	✗	✓

- **A12** – *Extreme fault conditions* – indicate if the method is evaluated considering extreme fault conditions, such as high-impedance faults or concurrent faults. The absence of this evaluation in reviewed papers reveals a gap for consideration in future studies;
- **A13** – *Hardware-in-the-loop validation* – indicates if the proposed method is validated with HIL experiments. The procedure of embedding a protection method in microcontrollers and conducting HIL experiments can demonstrate the applicability of a protection scheme.

It is common that every study presents strong remarks, but also some drawbacks or limitations. Therefore, Table 1 shows some of these limitations from a visual perspective by considering the revised papers compared to the present research. In addition, this comparative table highlights the importance and advantages of the proposed method in relation to existing research. In addition, some limitations were verified considering all the papers on extreme fault conditions and testing different optimization techniques. These specific aspects reflect the gaps that should be considered in future works.

III. THE PROPOSED PROTECTION STRATEGY

This section presents the rationale of the proposed strategy concerning design, tripping curves and coordination.

A. CONCEPTUAL DESIGN

Fig. 1a shows a flowchart with the interaction between the centralized protection system and the MG controller. It is important to note the MG's capability to operate flexibly. Thus, the MG protection schemes should consider these possible changes and adaptions to improve their response and dependability. Fig. 1b depicts a general MG and what information is needed by the protection to optimize its adjustments adaptively. The monitored information is: i) POI status to determine if the MG is operating in islanded or grid-connected mode; ii) DER status to determine if DERs are connected; iii) status of the switches to determine the operating MG topology; and iv) relay status to know if any self-healing action occurred. Having this information available to the MG controller allows verification of whether the protection settings align with the MG's operating conditions. If a change

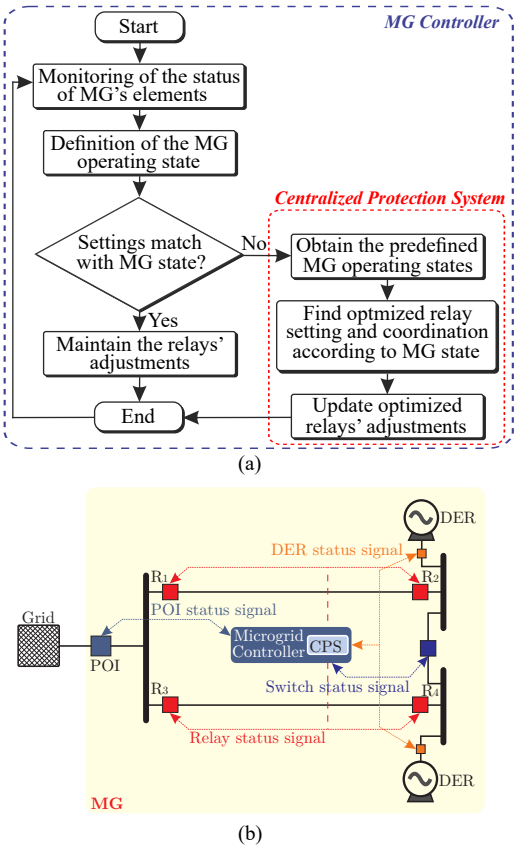

FIGURE 1. General rationale of the proposed MG protection approach.

This work is licensed under a Creative Commons Attribution 4.0 License. For more information, see https://creativecommons.org/licenses/by/4.0/

This article has been accepted for publication in IEEE Access. This is the author's version which has not been fully edited and content may change prior to final publication. Citation information: DOI 10.1109/ACCESS.2025.3565226

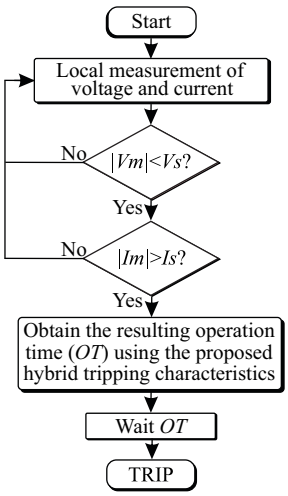

FIGURE 2. Flowchart of MG protection involving the online operation of relays using the proposed protection curves.

occurs, the centralized protection system provides predefined and optimized adjustments to the relays (offline process).

The directional overcurrent relays (DOCRs) continuously monitor voltage and current signals, locally and in a decentralized way. If the defined thresholds are reached, the DOCRs calculate the resulting operation times using the new hybrid tripping protection curve, presented in-depth in Section III-B.

Fig. 2 shows a flowchart of the DOCR operation of the MG (online process). It should be noted that when using DOCRs, voltage signals are intrinsically measured. Therefore, the proposed approach does not require additional measurements (e.g., harmonics and sequence components). Finally, backup relays can clear the fault if a primary relay fails, respecting a minimum coordination time interval (CTI). Therefore, primary relays are covered by backup relays when applicable, ensuring protection reliability. This aspect is addressed in Section III-C.

The flexibility of the proposed protection method is a key feature that enables it to adapt effectively to various MG configurations and operating conditions. As illustrated in Fig. 1, the centralized protection system interacts dynamically with the MG controller, monitoring critical parameters such as the POI status, DER connectivity, switch operating states, and relay actions. This allows the system to make predefined and optimized adjustments to the relays, ensuring that protection settings are aligned with the current operating mode of the MG, whether in islanded or grid-connected modes. Additionally, the DOCRs continuously monitor local voltage and current signals, allowing the protection system to operate without the need for extra measurements, as demonstrated in Fig. 2. This modular design ensures that the method remains reliable in a wide range of fault conditions and topologies, with primary relays backed up by secondary relays when necessary, ensuring a robust and adaptable protection scheme suitable for flexible MG environments.

While the proposed scheme uses a centralized system for updating relay settings, its implementation remains cost-effective compared to alternative solutions that rely on advanced measurement infrastructures, such as those based on phasor measurement units. The architecture leverages existing communication and control infrastructure in MGs, minimizing the need for additional investments. Moreover, since the centralized system does not perform real-time protection actions, high-speed communication is not required, further optimizing costs. This balance between adaptability, performance, and cost-efficiency makes the proposed approach a promising solution to improve MG protection.

B. PROPOSED HYBRID TRIPPING PROTECTION CURVE

This paper introduces a non-standard protection curve with hybrid tripping characteristics. The curve uses the voltage and current measurements acquired by the DOCRs to enable the time-counting process and determine the resulting operation time, as shown in (1):

$$OT = \left(\frac{A}{\left(\frac{I_f}{I_s}\right)^B - C} + D \right) \left(\left(E \frac{V_f}{V_s} \right)^\lambda + F \right) \times \zeta, \quad (1)$$

where OT is the operation time, and $\Lambda = [A, B, C, D, E, F, \lambda]$ is the set of constant values of the curve. I_f and I_s are the fault and setting current values, whose relation is M_I. Consequently, V_f and V_s are the fault and setting voltage values, whose relation is M_V. Moreover, ζ is a time multiplier setting, allowing coordination between MG protection devices.

Note from (1) that the proposed curve comprises two distinct components: one dependent on current signals and another on voltage signals. The latter provides a hybrid tripping characteristic, contributing to reducing the OT values. The constant set used in this paper was $\Lambda = [0.515; 0.020; 1.000; 0.114; 0.600; 0.030; \lambda]$. Similar to standardized IEC or ANSI curves, the constants A, B, C, D, and F are fixed and not treated as optimization variables, ensuring consistency in the protection characteristics.

Regarding λ, although it is also predefined, its value can be selected within the range $\tau = [2.5; 10]$ based on engineering criteria. As seen in (1), λ acts as an exponent in the voltage-dependent term, meaning that higher values result in shorter operation times. The preferred choice is $\lambda = 10$, provided that the coordination problem remains solvable. If any coordination constraint is violated, lower values of λ can be considered to restore feasibility while maintaining effective protection coordination. A global λ value is defined for all DOCRs, ensuring that no constraint violations occur while aiming to minimize MG protection response times. This approach guarantees that the proposed scheme remains both flexible and practical for real-world applications.

Fig. 3 depicts the general response of the proposed protection curve. In Fig. 3a, the impact of the voltage (M_V) and the current (M_I) during faults on the proposed curve considering

This work is licensed under a Creative Commons Attribution 4.0 License. For more information, see https://creativecommons.org/licenses/by/4.0/

This article has been accepted for publication in IEEE Access. This is the author's version which has not been fully edited and content may change prior to final publication. Citation information: DOI 10.1109/ACCESS.2025.3565226

$\zeta = 0.50$ and $\lambda = 2.5$ can be observed. Unlike the standard curves, when voltage during faults tends to low values, the *OT* values are likely to be lower. This response is promising for fault cases with low fault currents and moderate voltage drops. Fig. 3b shows the impacts of different values of ζ with $M_V = 0.50$ pu and $\lambda = 2.5$. As ζ is an adjustment variable, its modification enables the coordination and selectivity between the MG relays. In addition, Fig. 3c illustrates the variation in the tripping curves for different values of λ. As discussed, increasing λ leads to lower resulting *OT*s, enhancing the speed of operation. However, effective protection design is not solely about achieving the shortest possible operation times. It is crucial to maintain a balance between fast response and proper coordination among protection devices.

Fig. 4 shows the *OT*s regarding different voltage and current multiple pairs with $\zeta = 0.50$ and $\lambda = 2.5$. In Fig. 4a, some marked-up zones are highlighted. In Zone A, different from standard curves, when voltage during faults tends to low values, the *OT* values are likely to be lower even with low fault currents. In Zone B, voltage and current values contribute to a low *OT* of relays. Zone C comprises fault situations showing moderate voltage drops and current rises, resulting in moderate *OT*s. Moreover, in Zone D, there are fault cases where the voltage values are near the setting voltage, but the fault currents are high. As a result, even with a low drop in voltage, the *OT*s are low. Finally, Fig. 4b depicts the general response of the proposed curve when varying the ζ values.

The trip signal considering the proposed curve for a hypothetical MG low-fault-current scenario is presented in Fig. 5a. Even with the considerably low current values, as the voltage dropped considerably, the proposed protection curve enabled a fast protection trip at 0.1822 s. The fault inception occurred at 0.1 s of the simulation for this case. A comparison was made regarding the standard overcurrent (OC) curve, which presented a high operation time at 2.3295 s. Consequently, the trip was not illustrated in the graph, limited to a 0.4 s time-scale. The time-current-voltage characteristic proposed in [35] was also compared. This proposal led to a high operation time considering this specific case of a low-fault-current scenario, tripping at 0.9077 s. Considering the curve from [33], the trip occurred at 0.2278 s. The curve constants were the same, and the time multiplier setting was 0.3. In the curve from [35], another factor (K) was required and considered equal to 2.5 in this analysis.

A different scenario can be observed in Fig. 5b. In this situation, the voltage did not present a significant drop. This condition can make the protection curves, based on currents and voltages, more likely present high tripping times, as seen with the proposed curves of [33] and [35], whose trips occurred, respectively, at 0.5653 and 1.0478 s. In this example, the fault inception was at 0.05 s. The standard OC protection led to an operation at 0.6621 s due to the considerable current rise. Moreover, the proposed curve allowed the fastest trip at 0.2107 s. Finally, a particular fault case with islanded MG was used to represent scenarios with favorable conditions for

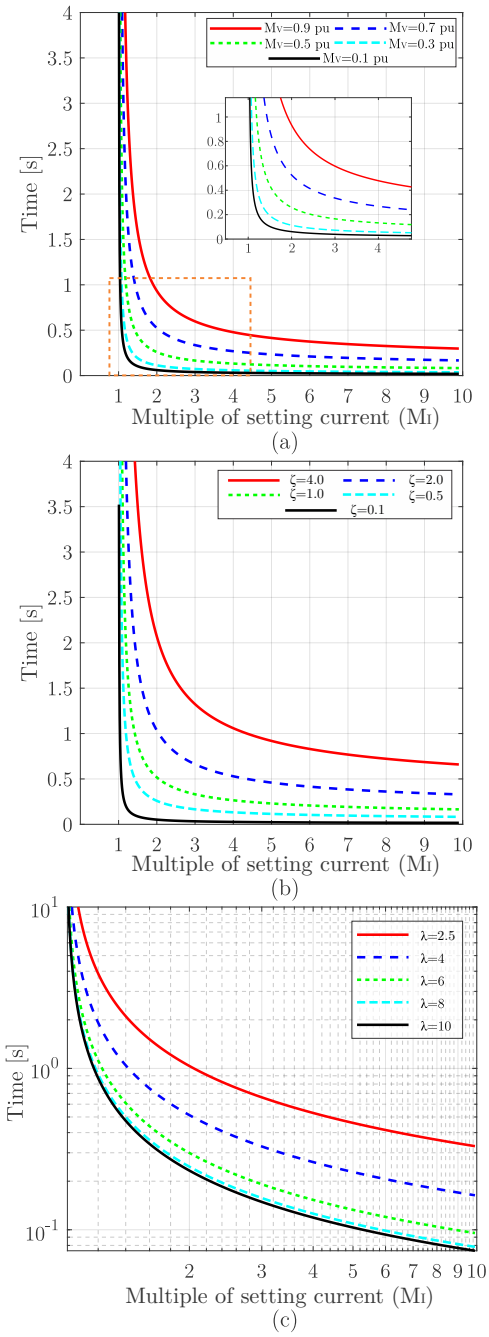

FIGURE 3. General response of the proposed curve: (a) Impact of voltage values with $\zeta = 0.5$ and $\lambda = 2.5$, (b) Impact of ζ values with $M_V = 0.5$ pu and $\lambda = 2.5$, and (c) Impact of λ values with $M_V = 0.5$ pu and $\zeta = 2.0$.

the protection curves, i.e., there was a great current rise and a great drop in voltage during the fault. All protection curves presented low *OT*s in this scenario, as depicted in Fig. 5c. The standard OC protection tripped at 0.7988 s; the curve from [35] tripped at 0.3704 s; the curve from [33] tripped at 0.2285 s; and the proposed curve tripped at 0.2191 s. In this example, the fault inception was at 0.20 s.

The promising performance of the proposed protection curve was evident considering the representative MG fault

This work is licensed under a Creative Commons Attribution 4.0 License. For more information, see https://creativecommons.org/licenses/by/4.0/

This article has been accepted for publication in IEEE Access. This is the author's version which has not been fully edited and content may change prior to final publication. Citation information: DOI 10.1109/ACCESS.2025.3565226

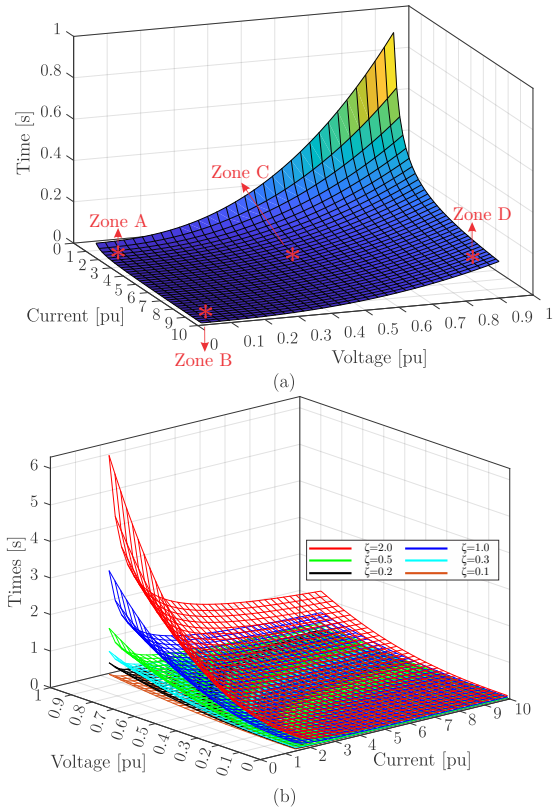

FIGURE 4. **Responses of the proposed curve for (a) $\zeta = 0.30$ and $\lambda = 2.5$, and (b) different values of ζ with $\lambda = 2.5$.**

cases listed. Even with different current and voltage behavior during the faults, the proposed curve presented low operation times compared with the standard OC protection and other non-standard protection curves. A common shortcoming of the existing non-standard curves was observed for the fault scenarios when the voltage presented a moderate drop and was near the set voltage value. This behavior was not observed when using the proposed non-standard curve. Subsequently, a discussion is presented regarding the coordination optimization problem of the protection considering the proposed curve. The coordination aspect is highly relevant, as it is not desired to obtain fast operation without coordination and selectivity.

C. PROTECTION COORDINATION PROBLEM

The parameters to be adjusted in the proposed curve are the variables β_g^{sc} of the optimal protection coordination (OPC). Thus, the objective function T^{sc} adopted for a scenario sc is:

$$\min \quad T^{sc}(\beta_g^{sc}) = \sum_{r=1}^{N_r}\sum_{f=1}^{N_f}(OT_{r,f}^{p} + \sum_{b=1}^{N_b} OT_{r,f}^{b}) \;\; \forall \;\; sc, \quad (2)$$

where $\beta_g^{sc} = [\mathrm{I}_{r,sc} \;\; \zeta_{r,sc}]$ is the group of variables of the optimization problem for a scenario sc; r represents the relay identifier, varying from 1 to N_r (number of relays); f is the fault identifier, varying from 1 to N_f (number of fault cases).

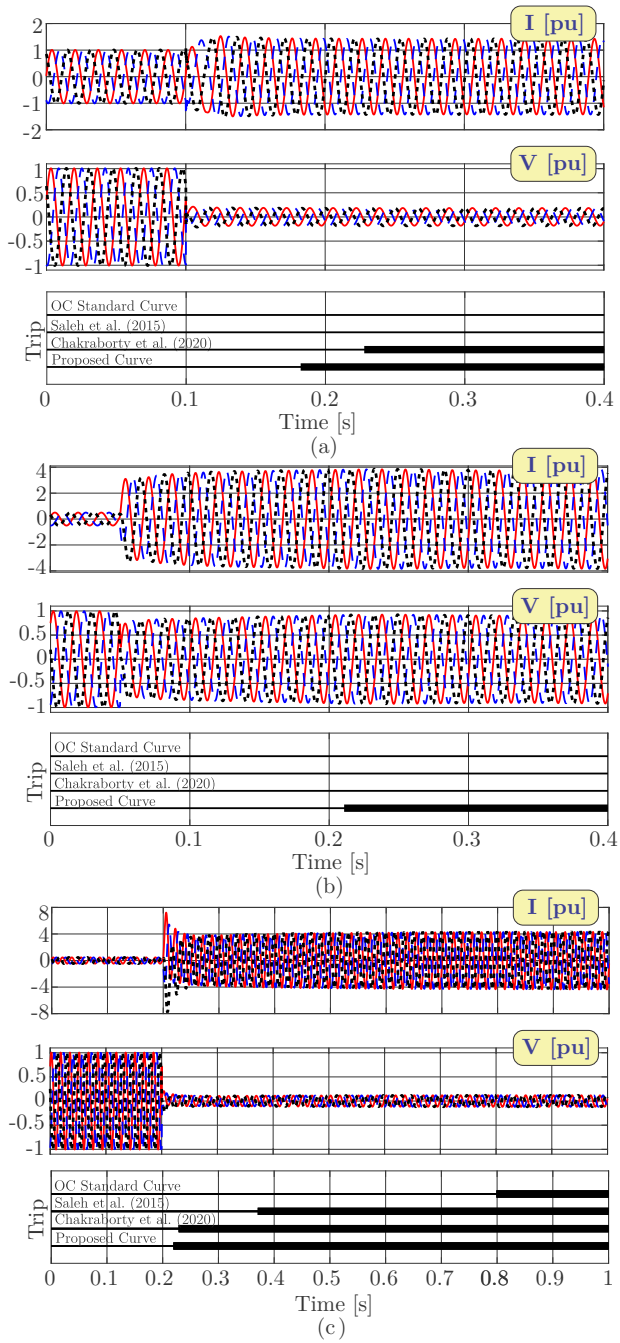

FIGURE 5. **Performance of different protection curves considering cases representing: (a) low-fault current scenarios, (b) scenarios with a minimum drop in voltage, and (c) favorable conditions for protection.**

Moreover, p indicates the primary relays, while b indicates the backup relays (varying from 1 to a total of N_b). Thus, OT is the relay's operation time, calculated according to (1). Finally, note that β_g^{sc} is comprised of $\mathrm{I}_{r,sc}$ and $\zeta_{r,sc}$. Thus, voltage setting V_s is addressed as a predetermined fixed value for all the relays and scenarios, simplifying the OPC. The resulting optimization problem is subject to the following constraints.

This work is licensed under a Creative Commons Attribution 4.0 License. For more information, see https://creativecommons.org/licenses/by/4.0/

This article has been accepted for publication in IEEE Access. This is the author's version which has not been fully edited and content may change prior to final publication. Citation information: DOI 10.1109/ACCESS.2025.3565226

1) Constraint set A – Coordination aspects

During the faults, both primary and backup relays are sensitized. Then, to obtain selectivity between the relays, the backup relays should present operation times that ensure preferential actions from the primary relays. To do this, for any fault, a minimum CTI should be respected by the backup relays, denoted as CTI_{min}. This value includes the circuit breaker opening time, a safety time and other minimum time differences and tolerances of the relays [40]. Therefore, the optimization problem should be solved considering the following constraints:

$$OT^{b}_{r,f} - OT^{p}_{r,f} \geq \text{CTI}_{min} \;\; \forall \;\; r,f, \tag{3}$$

where $OT^{b}_{r,f}$ is the operation time of backup relay r for a fault f, $OT^{p}_{r,f}$ is the operation time of primary relay r for the same fault f, and CTI_{min} is the minimum coordination interval time.

2) Constraint set B – Consideration on minimum operation time of relays

A second constraint set considers the minimum operation time of the relays. Although the optimization problem in this case aims to minimize the operation times of the relays, these devices have a minimum operation time consumed for their internal operations. Thus, this minimum operation time should be considered in the optimization problem. This assumption is represented next:

$$OT^{p}_{r,f}, OT^{b}_{r,f} \geq OT_{min} \;\; \forall \;\; r,f, \tag{4}$$

where $TO^{p}_{r,f}$ is the operation time of the primary relay r for a fault f, $OT^{b}_{r,f}$ is the operation time of the backup relay r for the fault f, and OT_{min} is the minimum operation time for any relay and fault.

3) Constraint set C – Consideration about ζ

The optimization variable ζ implies in direct changes on the response of the proposed hybrid characteristics, as discussed before. Thus, the main way for ensuring the coordination between the relays to vary ζ in the relays of the MG. Therefore, this set of constraints aims to determine an interval of interest for values of ζ, as described in the next equation.

$$\zeta^{min}_{r,sc} \leq \zeta_{r,sc} \leq \zeta^{max}_{r,sc} \;\; \forall \;\; r,sc, \tag{5}$$

where $\zeta^{min}_{r\,sc}$ is the minimum value of ζ of the relay r in the scenario sc, $\zeta^{min}_{r\,sc}$ is the adjusted value of ζ for the relay r in the scenario sc, and $\zeta^{max}_{r\,sc}$ is the maximum value of ζ for the relay r in the scenario sc.

4) Constraint set D – Consideration about I_s

Another constraint of the optimization problem considers the minimum and maximum values for the setting current of the relays, I_s. The setting current of a relay is selected here as a percentage (or multiple) of the nominal current of the protected area or line in a determined scenario. Thus, it can be ensured that the relays act only for faulty conditions. This constraint associated with I_s is determined as follows.

$$I^{min}_{r,sc} \leq I_{r,sc} \leq I^{max}_{r,sc} \;\; \forall \;\; r,sc, \tag{6}$$

where $I^{min}_{r,sc}$ is the minimum adjustment current of the relay r in the scenario sc, $I_{r,sc}$ is the selected adjustment current of the relay r in the scenario sc, and $I^{max}_{r,sc}$ is the maximum adjustment current of the relay r in the scenario sc. These currents could also be addressed as multiples of the respective load currents for a specific relay and scenario ($M_i = I_s/I_n$).

The resulting optimization problem is formulated as follows in 7a. It is important to observe that different constraint values could be assumed. Moreover, it can be observed that the formulated problem can be addressed as a non-linear-problem (NLP). Therefore, even considering the proposed hybrid and non-standard tripping characteristics and scenarios of MGs, the optimization problem formulation does not differ significantly from the conventional optimization problem formulated for distribution systems, which simplifies the proposed strategy.

$$\min \quad T^{sc}(\beta^{sc}_{g}) = \sum_{r=1}^{N_r}\sum_{f=1}^{N_f}(OT^{p}_{r,f} + \sum_{b=1}^{N_b} OT^{b}_{r,f}) \;\; \forall \;\; sc, \tag{7a}$$

s.t.

$$OT^{b}_{r,f} - OT^{p}_{r,f} \geq \text{CTI}_{min} \;\; \forall \;\; r,f, \tag{7b}$$

$$OT^{p}_{r,f}, OT^{b}_{r,f} \geq OT_{min} \;\; \forall \;\; r,f, \tag{7c}$$

$$\zeta^{min}_{r,sc} \leq \zeta_{r,sc} \leq \zeta^{max}_{r,sc} \;\; \forall \;\; r,sc, \tag{7d}$$

$$I^{min}_{r,sc} \leq I_{r,sc} \leq I^{max}_{r,sc} \;\; \forall \;\; r,sc. \tag{7e}$$

As the adjustment group β^{sc}_{g} is optimized for each operating scenario, it is important to identify the current MG operation. Thus, when necessary, the optimized adjustments should be updated in the relays. Although this was not a focus of the present paper, existing strategies could be properly employed [36], [37]. Finally, it is worth mentioning that from this formulation, the OPC considers the proposed hybrid tripping characteristics for the MG context. In order to solve this problem, the Matlab optimization toolbox with the simple gradient descent algorithm was used, demonstrating the simplicity of the approach. The constraint tolerance, step tolerance, and optimality tolerance were established as 1E-10. In future studies, other optimization algorithms could be tested to solve the OPC.

D. DEFINING BOUNDARY CONDITIONS

Regarding the formulated OPC, CTI_{min} was defined as 200 ms, and the OT_{min} as 30 ms. The optimization variable $\zeta_{r,sc}$ was bounded from 0.01 to 20. Moreover, $I_{r,sc}$ boundaries were 1.2 and 2.0 pu of the nominal load current for each scenario. Finally, the $V_{r,sc}$ was defined as 0.88 pu for all the relays and scenarios. This value was based on the IEEE Std. 1547 [39], which points out that voltages on island areas could drop to 0.88 pu in a healthy operation. It should be highlighted

This work is licensed under a Creative Commons Attribution 4.0 License. For more information, see https://creativecommons.org/licenses/by/4.0/

This article has been accepted for publication in IEEE Access. This is the author's version which has not been fully edited and content may change prior to final publication. Citation information: DOI 10.1109/ACCESS.2025.3565226

that other boundaries' values and settings could be carefully implemented by analyzing their impacts on the coordination and protection response. Thus, note that all the boundaries are not constrained to the MG tested in this paper, i.e., the proposed method can be extended to other MGs.

E. CONSIDERATIONS ON COMMUNICATION DELAY AND LIMITATIONS OF THE METHOD

Regarding the communication between protective devices and the adjustment update, it can be found in the literature that the message exchange times between protective devices are relatively low. In [41], it was pointed out that the delay in sending and receiving messages is approximately $4, 9\ \mu$s/km. Furthermore, considering the IEC61850 context, GOOSE messages between two or more devices presented a maximum transmission delay of 4 ms, as mentioned in [42]. Thus, the existing communication infrastructure of an MG enables the safe adjustment update of the proposed protection. Finally, it is worth emphasizing that operation during faults occurs locally, and only the update of the relays' settings depends on this communication infrastructure, improving the protection dependability.

It is important to highlight that the proposed method was not designed to address extreme faults specifically, such as high impedance faults. As shown in Table 1, none of the reviewed studies on MG protection schemes explicitly consider this type of fault, given its unique characteristics and detection challenges. Consequently, this limitation is not exclusive to the proposed method but rather a general constraint in MG protection strategies. Nevertheless, an additional protection module could be integrated into the proposed scheme to specifically detect high impedance faults. For instance, in [43], the authors presented a method leveraging image classification techniques to identify high impedance faults in MGs, which could serve as a complementary approach.

IV. SIMULATION RESULTS

This section introduces the test MG, outlines the operational scenarios, and provides a detailed discussion of the simulation results.

A. TEST MICROGRID DESCRIPTION

The test MG, depicted in Fig. 6, was implemented in PSCAD to evaluate the proposed protection scheme. This MG was based on a CIGRE benchmark for integrating renewable DERs into the grid [44]. The delimited area to the MG, illustrated in Fig. 6, has a load of 4.32 MW and 1.43 Mvar with a nominal voltage of 20 kV. This system's electrical parameters can be found in [44]. The MG comprises a synchronous-based DG (5 MVA) at node 5 and a type IV wind turbine generator (2 MW) integrated with a battery energy storage system (1 MW) at node 8 for wind power smoothing purposes. In this MG, islanding occurs when the POI switch is opened. Moreover, the MG has a normally-open switch (S) that allows self-healing actions by interconnecting nodes 6 and 7. The synchronous-based DG represented a dispatchable

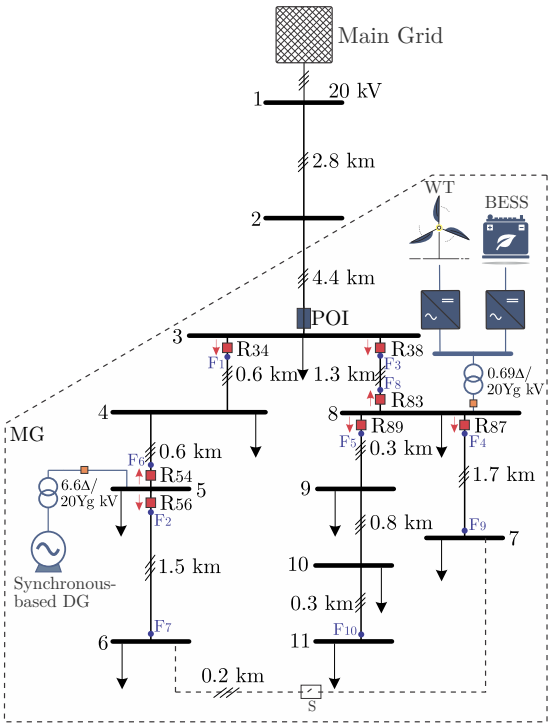

FIGURE 6. Test MG used for evaluation of the proposed protection.

source and operated in grid-following control mode for the grid-connected operating mode. In addition, this DG operated in grid-forming control mode in islanded operating mode, providing frequency and voltage references to the MG. In addition, a fault current limitation of 1.5 pu was considered in the wind turbine generator control. Finally, note that MG is protected using seven DOCRs with the hybrid tripping characteristics proposed in this paper.

B. OPERATION SCENARIOS OF MICROGRID AND FAULT CONDITIONS

The robustness of the proposed protection strategy was evaluated through simulations involving both symmetrical and asymmetrical faults (PPP - three-phase faults, PP-G - double-line-to-ground faults, PP - double-line faults, and P-G - single-line-to-ground faults) across seven distinct operating scenarios of the MG. These scenarios (*sc*) were designed to capture a variety of operating conditions and included: (1) islanded MG with all the DERs in operation; (2) islanded MG with only synchronous-based DG; (3) grid-connected MG with all the DERs in operation; (4) grid-connected MG with only synchronous-based DG; (5) grid-connected MG without any DER; (6) islanded MG with self-healing, where line 3-8 was isolated and switch S was closed; and (7) islanded MG with self-healing, where line 3-5 was isolated and switch S was closed.

For each scenario, the different fault types, including both symmetrical and asymmetrical faults (PPP, PP-G, PP, P-G), were simulated, and fault resistances ranging from 0 Ω to 20 Ω, in increments of 2.5 Ω, were considered. The simu-

This work is licensed under a Creative Commons Attribution 4.0 License. For more information, see https://creativecommons.org/licenses/by/4.0/

This article has been accepted for publication in IEEE Access. This is the author's version which has not been fully edited and content may change prior to final publication. Citation information: DOI 10.1109/ACCESS.2025.3565226

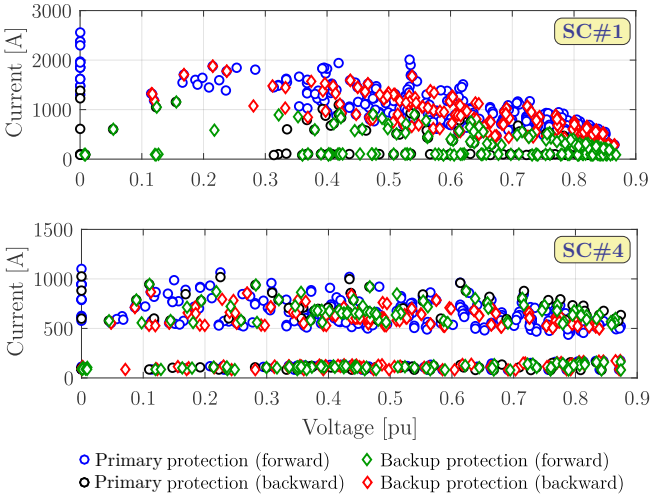

FIGURE 7. Voltage and current data considering scenarios 1 and 4.

lations assessed faults at both near-end and far-end locations to ensure that the protection settings provided reliable performance under varying conditions. Based on the operating scenario, specific relays were either activated or deactivated. For example, in Scenario 6 (an islanded operation – POI switch is open), where line 3-8 was isolated, relays R38, R83, and R34 were intentionally disabled to reflect the altered network configuration. To illustrate the data obtained from the simulated faults, Fig. 7 shows the voltage and current pairs for scenarios 1 and 4. As expected, a significant difference is found in the fault behavior of MG when operating in islanded or grid-connected modes. This behavior highlights the need for the protection system to be adaptable, ensuring reliable performance across all operating scenarios. The impact of these variations is further evident in the time-domain current waveforms shown in Fig. 8, which also reveal how fault characteristics differ depending on the MG's operating mode.

C. RESULTING OPTIMIZED ADJUSTMENTS

The resulting adjustments of the relays considering all the analyzed scenarios are shown in Table 2. A set current I_s of 1.2 pu was obtained for all relays. Moreover, as previously mentioned, a setting voltage V_s of 0.88 pu was also adopted for all relays. It is important to observe that, opposite to the behavior of the base voltage, the base current differs for each relay and scenario. Fig. 9 shows the general behavior of ζ values considering all the scenarios.

This graph presents box-plots for all relays, illustrating the ζ variation depending on the scenario to allow coordination between relays and fast response with adaptability. In the analyzed MG and its scenarios, $\lambda = 10$ resulted in a faster response without jeopardizing coordination, as discussed next. Thus, this constant value was used in (1) for all relays.

Moreover, Figs. 10 and 11 illustrate the convergence behavior of the OPC considering both islanded and grid-connected operating modes. The rapid convergence of the method, its feasibility in final iteration, and the final values of the optimization variables can be observed.

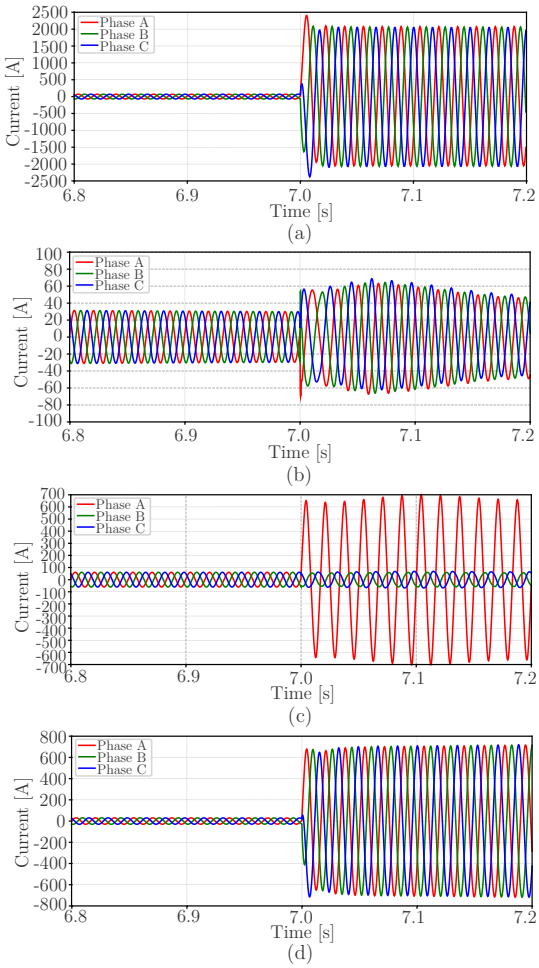

FIGURE 8. Current waveforms during faults under different operating conditions: (a) solid ABC fault in primary of R34, considering a grid-connected operating mode; (b) 15 Ohm ABC fault in primary of R83, considering an islanded operating mode; (c) 5 Ohm AG fault in primary of R34, considering a grid-connected operating mode; and (d) 15 Ohm ABC fault in R38 considering islanded operating mode.

TABLE 2. Optimized adjustments considering the analyzed scenarios

	$\zeta^1_{s,r}$	$\zeta^2_{s,r}$	$\zeta^3_{s,r}$	$\zeta^4_{s,r}$	$\zeta^5_{s,r}$	$\zeta^6_{s,r}$	$\zeta^7_{s,r}$
R34	4.1248	-	6.8732	6.7578	8.3451	-	-
R54	14.9823	9.6611	11.2198	11.0153	-	0.8222	-
R56	1.3850	1.3195	1.6306	1.6128	1.4342	8.6275	9.4744
R38	8.8767	6.3706	10.6820	8.5501	7.7339	-	-
R83	7.8677	-	16.8706	-	-	-	1.3010
R89	1.0221	0.9478	1.2503	1.2258	1.1203	1.0032	0.9680
R87	1.9021	1.8400	2.0927	2.0722	1.9840	0.5503	0.4895

D. OVERALL ANALYSIS OF THE PROTECTION

The resulting primary and backup protection OTs, and the verified CTIs were analyzed considering all fault cases and MG operating scenarios. It is important to highlight that there

This work is licensed under a Creative Commons Attribution 4.0 License. For more information, see https://creativecommons.org/licenses/by/4.0/

This article has been accepted for publication in IEEE Access. This is the author's version which has not been fully edited and content may change prior to final publication. Citation information: DOI 10.1109/ACCESS.2025.3565226

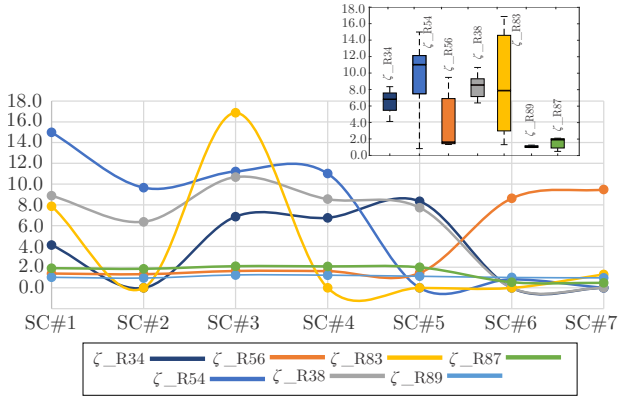

FIGURE 9. Behavior of the setting ζ values of the relays considering all the scenarios of the MG.

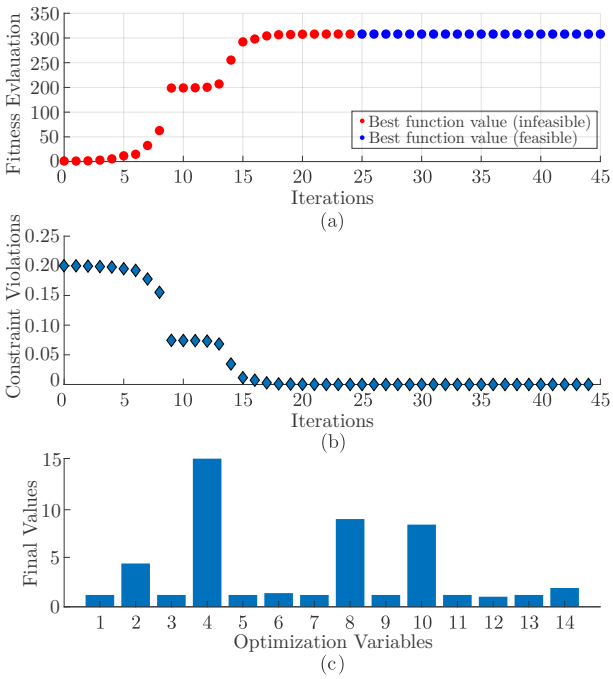

FIGURE 10. Convergence behavior of the OPC considering an islanded scenario.

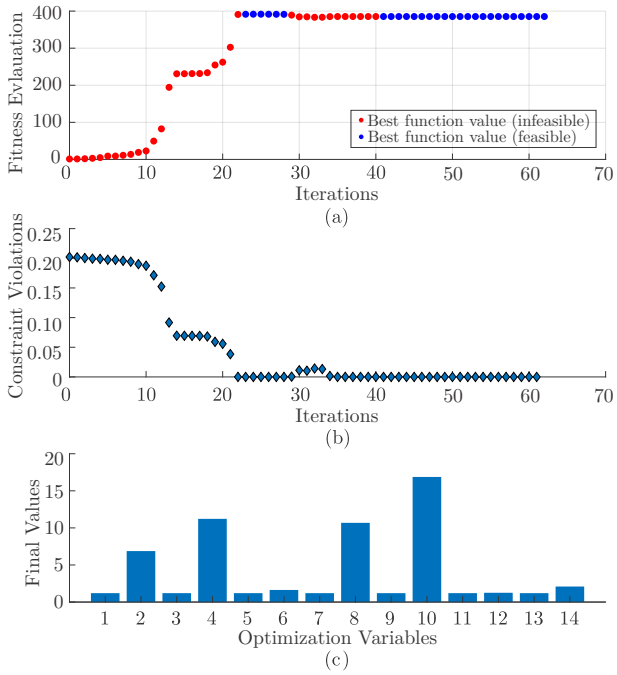

FIGURE 11. Convergence behavior of the OPC considering a grid-connected scenario.

were no constraint violations in any analyzed scenario, showing that the proposed hybrid tripping characteristics allow a feasible OPC solution. Table 3 shows a complete statistical analysis of the obtained OT_p, OT_b, and CTI values by presenting their minimum, maximum, and percentile values. In this table, P_{10} indicates the 10th percentile, P_{20} the 20th percentile, and so on. Thus, a comprehensive overview of the proposed protection's performance can be obtained by considering a variety of operational scenarios.

Regarding the statistical analysis, it can observed that the proposed protection was fast, selective, and dependable. Considering all the OT_p values, a minimum time of 0.0300 s was found, which is the minimum operation time predefined as a boundary condition. The maximum observed OT_p was 2.6843 s, while 95% of the OT_p values were lower than 0.9638 s. In terms of OT_b, the minimum time was 0.2300 s, also respecting the minimum boundary condition. The maximum time was 2.6929 s, where the P_{95} was lower than 1.2017 s. The CTI_{min} of 0.2 s was also insured, which corresponded to the minimum and maximum values of CTI of 0.2000 s and 2.3311 s, respectively. The P_{95} of CTI was lower than 1.2017 s.

The broad statistical view of the protection performance indicates that the proposed protection yielded fast response times without disregarding the coordination aspect. In grid-connected operation (scenarios 3 and 4), even presenting moderate maximum values for OT_p, OT_b, and CTI, the 95th percentile values were substantially lower than the observed maximum values. This can be clearly seen in Fig. 12, which shows a heatmap with different percentiles considering the OT_p, OT_b, and CTI values for all the investigated scenarios. To provide additional clarity, operation times exceeding 1 second are highlighted in Table 3. It is important to note that the proposed non-standard protection curve was designed to ensure rapid tripping for high fault currents, while longer operation times occur in low-magnitude faults, close to nominal conditions. Considering the Joule integral principle, these cases do not compromise the thermal withstand capability of the equipment. This ensures that the method maintains a balance between fast operation and system security.

This work is licensed under a Creative Commons Attribution 4.0 License. For more information, see https://creativecommons.org/licenses/by/4.0/

This article has been accepted for publication in IEEE Access. This is the author's version which has not been fully edited and content may change prior to final publication. Citation information: DOI 10.1109/ACCESS.2025.3565226

TABLE 3. Statistical data of the OT_p, OT_b and CTIs (in seconds)

		Min.	P_{10}	P_{20}	P_{30}	P_{40}	P_{50}	P_{60}	P_{70}	P_{80}	P_{85}	P_{90}	P_{95}	Max.
SC#1	OTp	0.0300	0.0320	0.0334	0.0350	0.0385	0.2484	0.2693	0.3870	0.4715	0.4941	0.5138	0.5437	0.7615
	OTb	0.2300	0.2468	0.2540	0.2621	0.2708	0.2956	0.4272	0.4721	0.5000	0.5130	0.5390	0.6181	0.8046
	CTI	0.2000	0.2070	0.2171	0.2203	0.2250	0.2294	0.2352	0.2431	0.2532	0.5130	0.2727	0.6181	0.4108
SC#2	OTp	0.0300	0.0316	0.0324	0.0333	0.0344	0.0356	0.1310	0.2663	0.3557	0.4628	0.5128	0.5425	0.6130
	OTb	0.2300	0.2482	0.2634	0.2715	0.2768	0.2827	0.2949	0.4577	0.5155	0.5330	0.5525	0.5731	0.6294
	CTI	0.2000	0.2148	0.2234	0.2323	0.2380	0.2431	0.2484	0.2548	0.2648	0.5330	0.2787	0.5731	0.3242
SC#3	OTp	0.0300	0.0329	0.0356	0.0391	0.0476	0.2537	0.3256	0.4808	0.7703	0.8140	0.8784	0.9638	**2.6834**
	OTb	0.2300	0.2513	0.2704	0.2961	0.3352	0.3799	0.5617	0.7706	0.8394	0.9017	0.9507	**1.1709**	**2.6929**
	CTI	0.2000	0.2177	0.2353	0.2534	0.2822	0.3117	0.3618	0.4596	0.5229	0.9017	0.6311	**1.1709**	**2.3311**
SC#4	OTp	0.0300	0.0323	0.0343	0.0368	0.0410	0.1316	0.2683	0.3433	0.4642	0.5527	0.6445	0.8748	**1.9978**
	OTb	0.2300	0.2516	0.2707	0.2950	0.3213	0.3581	0.4060	0.5062	0.6239	0.7093	0.8605	**1.2017**	**2.0403**
	CTI	0.2000	0.2189	0.2345	0.2546	0.2757	0.2979	0.3342	0.3675	0.4613	0.7093	0.6601	**1.2017**	**1.6327**
SC#5	OTp	0.0300	0.0319	0.0330	0.0344	0.0359	0.0384	0.1333	0.2768	0.3131	0.3346	0.3603	0.4101	0.4994
	OTb	0.2303	0.2531	0.2680	0.2827	0.2957	0.3103	0.3254	0.3446	0.3654	0.3816	0.4090	0.4575	0.5166
	CTI	0.2003	0.2216	0.2343	0.2486	0.2624	0.2752	0.2911	0.3077	0.3286	0.3816	0.3725	0.4575	0.4755
SC#6	OTp	0.0300	0.0325	0.0340	0.0350	0.0365	0.0380	0.0410	0.0452	0.2382	0.2437	0.2523	0.2614	0.3032
	OTb	0.2300	0.2413	0.2476	0.2488	0.2519	0.2535	0.2605	0.2634	0.2706	0.2779	0.2856	0.3012	0.3106
	CTI	0.2000	0.2093	0.2146	0.2151	0.2171	0.2189	0.2242	0.2272	0.2339	0.2779	0.2475	0.3012	0.2702
SC#7	OTp	0.0300	0.0311	0.0322	0.0329	0.0337	0.0348	0.0363	0.0392	0.2348	0.2412	0.2478	0.2563	0.2820
	OTb	0.2305	0.2376	0.2419	0.2458	0.2464	0.2480	0.2521	0.2567	0.2590	0.2609	0.2659	0.2715	0.2862
	CTI	0.2000	0.2060	0.2101	0.2119	0.2130	0.2140	0.2187	0.2215	0.2231	0.2609	0.2278	0.2715	0.2470

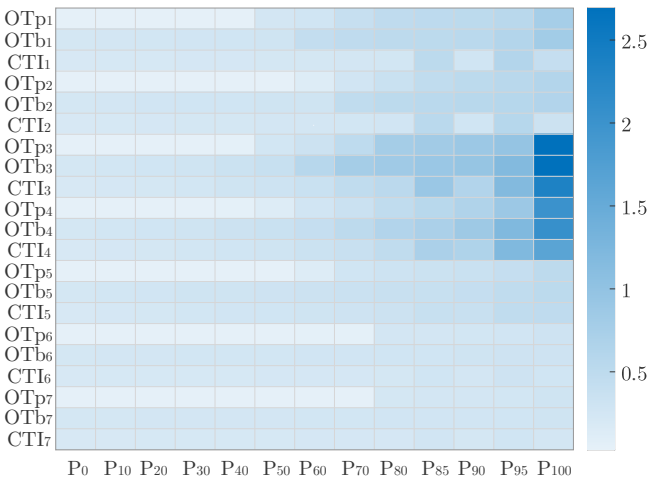

FIGURE 12. Heatmap with different percentiles for primary and backup operation times and CTIs considering all the investigated scenarios.

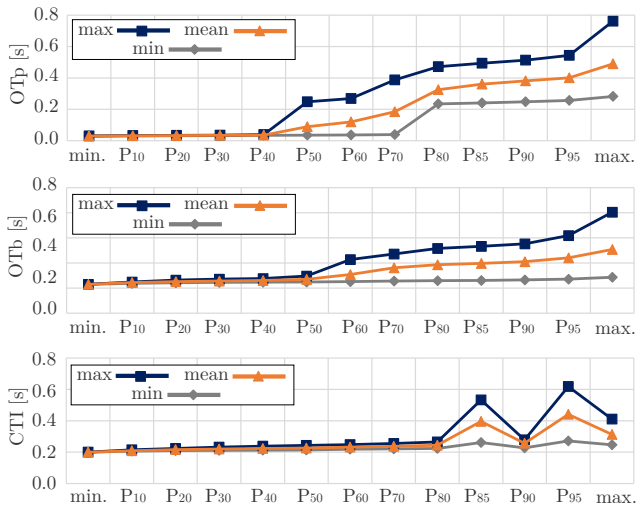

FIGURE 13. Statistical data for the obtained OT_p, OT_b, and CTI values considering islanded scenarios.

E. OPERATION TIMES AND COORDINATION TIME INTERVALS IN ISLANDED MODE

The scenarios corresponding to the MG islanded operation mode were 1, 2, 6, and 7. The performance of the protection for these situations can be observed in Table 3. Nevertheless, to better assess these results, Fig. 13 depicts general statistical information considering only islanded scenarios in terms of OT_p, OT_b and CTI values. The graphs show the minimum, mean and maximum values among the verified percentiles shown in Table 3, thus verifying the overall performance of the protection regarding islanded operation modes. The results indicated a fast protection response with a fast backup operation. The maximum OT_p observed in the islanded scenarios was 0.7615 s, in which more than 95% of the trips (95th percentile) ocurred at times lower than 0.5437 s. Moreover, a narrow range is evident when examining the CTI values.

F. OPERATION TIMES AND COORDINATION TIME INTERVALS IN GRID-CONNECTED MODE

Fig. 14 depicts general statistical information regarding only grid-connected MG scenarios. Even with moderate values observed in maximum OT_p, OT_b, and CTIs, all the values are substantially decreased in the 95th percentile. For example, the mean values between the grid-connected scenarios for the 90th percentile of OT_p, OT_b, and CTI were 0.6277 s, 0.7401 s, and 0.5546 s, respectively. Therefore, considering the grid-connected operation mode, the proposed protection presented adequate coordination between the relays and low OT values.

This work is licensed under a Creative Commons Attribution 4.0 License. For more information, see https://creativecommons.org/licenses/by/4.0/

This article has been accepted for publication in IEEE Access. This is the author's version which has not been fully edited and content may change prior to final publication. Citation information: DOI 10.1109/ACCESS.2025.3565226

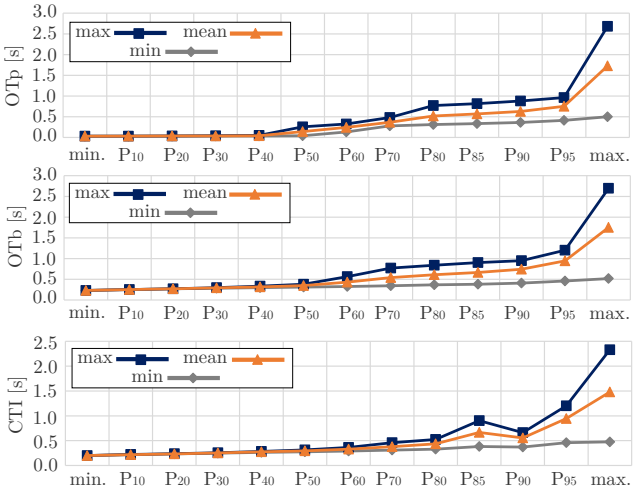

FIGURE 14. Statistical data for the obtained OT_p, OT_b, and CTI values considering grid-connected scenarios.

G. FINAL PERFORMANCE ANALYSIS

The final performance analysis consisted of a statistical evaluation of all results obtained from the proposed protection scheme. Regarding primary protection operation times, the minimum tripping time was 0.030 s, the median time was 0.0415 s, the 90th percentile operation time was 0.5308 s, and the maximum time was 2.6834 s. Therefore, in 90% of all faults, the protection system operated within 0.5308 s. All faults were cleared and any malfunction was observed.

For backup protection, the minimum operation time was 0.2300 s, the median time was 0.2996 s, the 90th percentile time was 0.6945 s, and the maximum time was 2.6929 s. For all applicable cases, backup protection operated correctly.

Finally, the coordination time intervals had a maximum value of 2.3311 s, with 95% of cases occurring within 0.5953 s. It is important to note that the faults analyzed covered various operating conditions (in islanded and grid-connected modes) that could compromise protection performance, affecting operation times, coordination times, and selectivity. However, the proposed protection scheme demonstrated reliable performance by effectively balancing fast operation and selectivity with correct operation for all cases.

V. HARDWARE-IN-THE-LOOP EVALUATION

To investigate the applicability of the proposed strategy, the hybrid tripping characteristics with optimized adjustments were embedded and evaluated in hardware for real-time operation, as presented next. Although this experiment does not constitute a physical evaluation of the proposed method in a real-world MG, the successful integration of the strategy into hardware and its validation through HIL testing provide valuable insights into its real-time performance. HIL experiments consider many of the challenges associated with real-time execution, such as processing delays and computational load of embedded algorithms. By embedding the hybrid tripping characteristics into a microcontroller and subjecting it to these real-time constraints, we can observe how well the protection strategy adapts to dynamic conditions. Therefore, while this validation does not replace real-world deployment, it provides assurance that the proposed protection system can function reliably when implemented in actual hardware environments.

A. EXPERIMENTAL SETUP

Fig. 15 illustrates the general schematic of the used testbed, indicating the closed loop between the RTDS and the microcontroller units (MCUs). The MCUs were the F28379D launchpads from Texas Instruments, representing the relays across the MG. The choice of this microcontroller was driven mainly by successful implementations by other researchers for embedded algorithm testing. Moreover, its low cost and simplicity were key factors in the decision. Demonstrating the method's effectiveness even with a low-cost microcontroller provides a strong indication that the proposed approach could perform well in real-world applications.

The high electromagnetic interference within the laboratory motivated the design of passive first-order anti-aliasing filters with $R = 680\ \Omega$ and $C = 680$ nF, resulting in a cut-off frequency near 360 Hz. In MCUs, the analog-to-digital converter was a 12-bit with a sampling frequency of 1,920 Hz. This sampling frequency (32 samples/power cycle) aligns with commercial relays, such as the SEL-751 relay from Schweitzer Engineergin Laboratories [45]. As a result, each MCU produced a digital signal (protection trip) that was injected back into the RTDS, closing the loop. In the tests performed, the adjustments shown in Table 2 were considered when embedding the curve in MCUs.

In the experiments, the simulated voltages and currents were converted to analog voltage signals ranging from 0

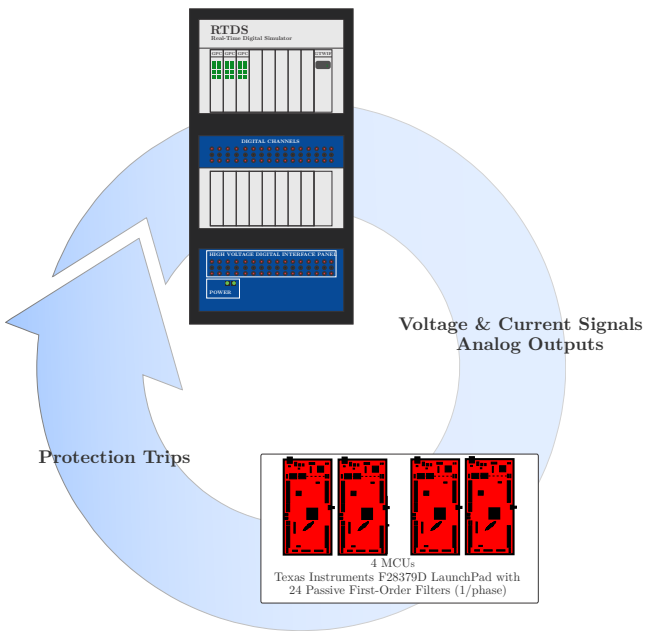

FIGURE 15. General schematic of the used testbed.

This work is licensed under a Creative Commons Attribution 4.0 License. For more information, see https://creativecommons.org/licenses/by/4.0/

This article has been accepted for publication in IEEE Access. This is the author's version which has not been fully edited and content may change prior to final publication. Citation information: DOI 10.1109/ACCESS.2025.3565226

to 3 V to properly interface with the MCUs. This range was chosen considering the nominal voltage of the selected MCUs, which is 3.3 V [46]. Consequently, the analog output voltage of RTDS was set between 0 and 3 V. It is worth mentioning that the cables used between the RTDS and the filters were shielded, featuring four twisted pairs plus a ground conductor per cable. They consisted of three layers: a polyethylene inner layer, a PVC intermediate layer, and an aluminum outer shielding. Twisted pairs helped minimize interference. In total, the setup included 24 analog outputs from the RTDS (six signals per MCU), 24 passive filters, and three cables connecting the RTDS to the filters and MCUs. Fig. 16 illustrates the experimental setup, highlighting the RTDS rack (left) and MCUs.

B. EXPERIMENTAL RESULTS

In the experiments, the protection response was evaluated for eight fault cases. These fault cases were selected from the ones presented in Section IV-B, as described next:

- Test I: 5 Ω single-line-to-ground fault in path 3–5 considering scenario 3 (grid-connected operating mode);
- Test II: 10 Ω double-line-to-ground fault in path 8–7 considering scenario 4 (grid-connected operating mode);
- Test III: solid three-phase fault in path 3–5 considering scenario 1 (islanded operating mode);
- Test IV: 20 Ω single-line-to-ground fault in path 8–11 considering scenario 1 (islanded operating mode);
- Test V: 20 Ω double-line fault in path 5–6 considering scenario 4 (grid-connected operating mode);
- Test VI: 20 Ω single-line-to-ground fault in path 8–11 considering scenario 4 (grid-connected operating mode);
- Test VII: 15 Ω single-line-to-ground fault in path 3–8 considering scenario 2 (islanded operating mode);
- Test VIII: 10 Ω three-phase fault in path 5–8 considering scenario 6 (islanded operating mode with self-healing).

Figs. 17 to 24 show the experimental results. These graphs display the analog current and voltage signals interpreted by MCUs in the 0–3 V range. In addition, the corresponding protection trips for each relay are also shown. Table 4 shows a comparison between the experimental and simulated results, where it can be observed that the experimental results (protection trips) were close to the simulated ones.

TABLE 4. Summary of the experimental results and a general comparison with simulated results (trips in seconds)

Test	Relay	Software	Hardware	Difference
I (5 Ω AG fault)	R34	0.301	0.323	0.023
	R54	0.555	0.596	0.041
	R83	0.823	0.887	0.064
II (10 Ω ABg fault)	R87	0.034	0.076	0.041
	R38	0.313	0.340	0.027
III (solid ABC fault)	R34	0.369	0.374	0.005
	R83	0.624	0.649	0.025
	R54	0.500	0.526	0.026
IV (5 Ω AG fault)	R89	0.041	0.074	0.032
	R38	0.295	0.323	0.028
V (20 Ω AB fault)	R56	0.039	0.073	0.034
	R34	0.404	0.416	0.012
VI (20 Ω Ag fault)	R89	0.049	0.072	0.023
	R38	0.415	0.424	0.010
VII (15 Ω Ag fault)	R38	0.266	0.299	0.032
	R54	0.532	0.569	0.037
VIII (10 Ω ABC fault)	R87	0.045	0.081	0.036
	R56	0.261	0.286	0.025
All the tests			*Mean Difference* [s]	0.029
			Maximum Difference [s]	0.064
			Minimum Difference [s]	0.005

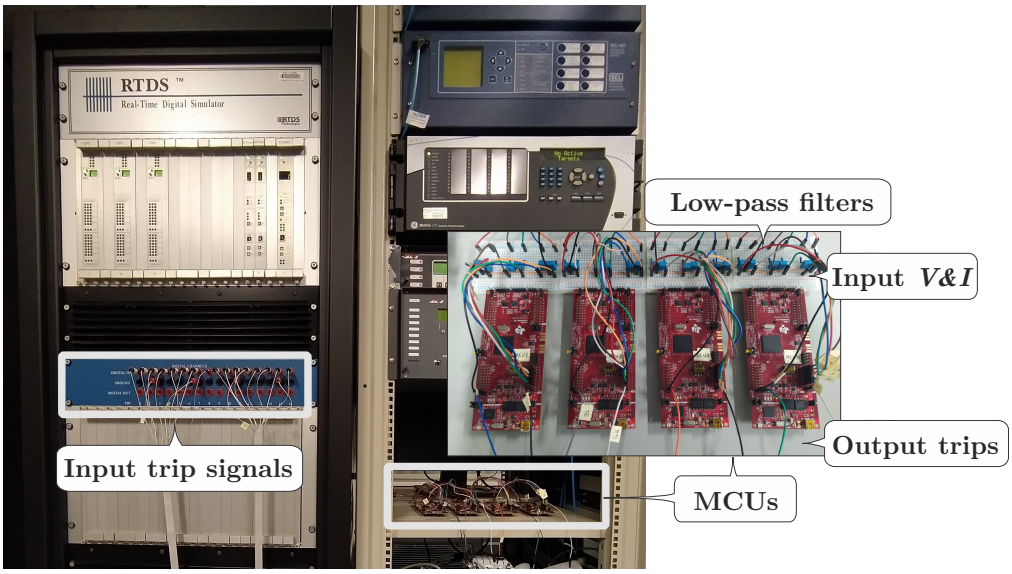

FIGURE 16. Experimental setup with RTDS and MCUs.

This work is licensed under a Creative Commons Attribution 4.0 License. For more information, see https://creativecommons.org/licenses/by/4.0/

This article has been accepted for publication in IEEE Access. This is the author's version which has not been fully edited and content may change prior to final publication. Citation information: DOI 10.1109/ACCESS.2025.3565226

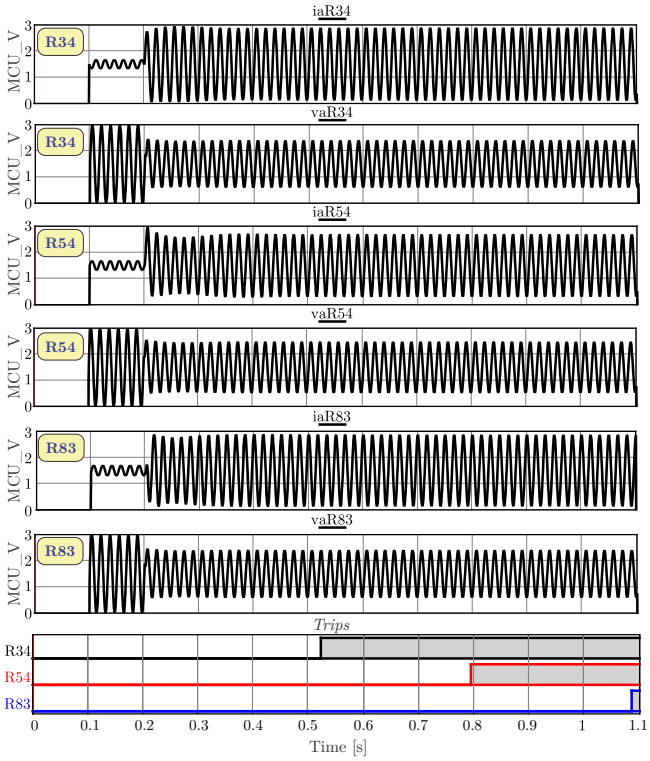

FIGURE 17. Real-time experiment I – 5 Ohm single-line-to-ground fault in path 3–5 considering scenario 3 (grid-connected operating mode).

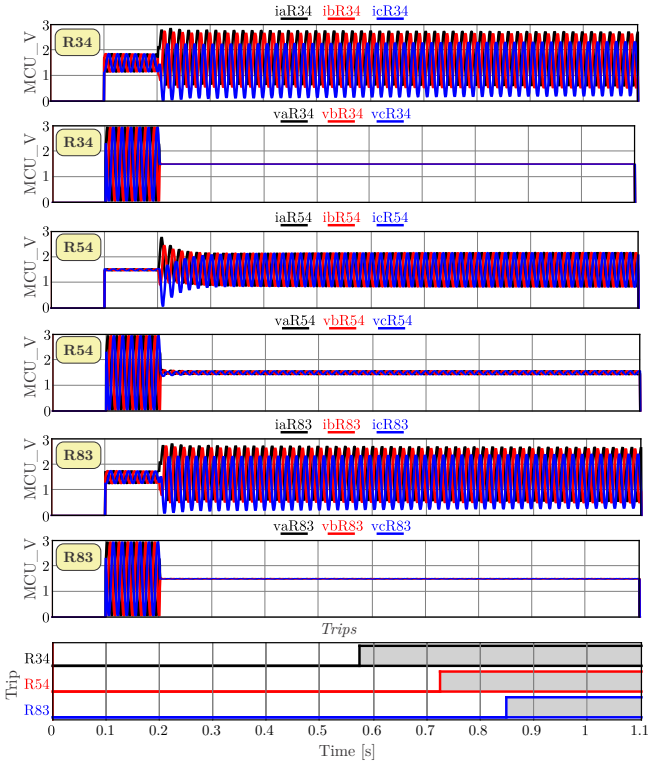

FIGURE 19. Real-time experiment III – solid three-phase fault in path 3–5 considering scenario 1 (islanded operating mode).

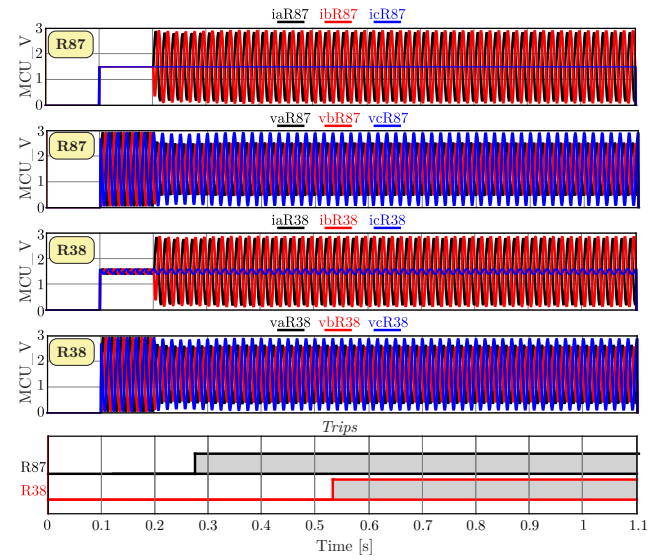

FIGURE 18. Real-time experiment II – 10 Ohm double-line-to-ground fault in path 8–7 considering scenario 4 (grid-connected operating mode).

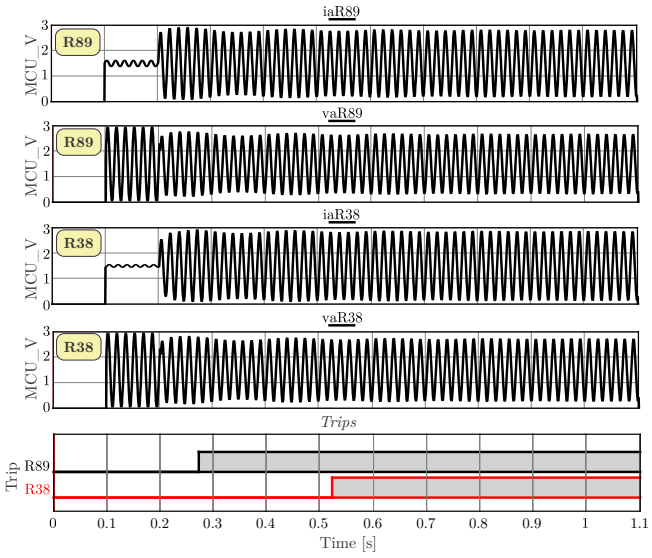

FIGURE 20. Real-time experiment IV – 20 Ohm single-line-to-ground fault in path 8–11 considering scenario 1 (islanded operating mode).

In addition, Table 4 also presents the mean, maximum, and minimum differences considering all the tests performed. Regarding the CTIs, the mean, maximum, and minimum differences observed experimentally were 0.017 s, 0.004 s, and 0.041 s, respectively. Therefore, the experimental results confirm that the proposed protection presented fast operation and good selectivity. Finally, it should be emphasized that the proposal hardware is simple to be embedded in low-cost MCUs.

Finally, it is important to observe that the experimental results demonstrated that the proposed method operates within acceptable deviation margins when compared to the SEL-751 commercial relay [45]. While the manufacturer specifies an accuracy variation of ± 1.5 cycles $\pm 4\%$ of the absolute value,

This work is licensed under a Creative Commons Attribution 4.0 License. For more information, see https://creativecommons.org/licenses/by/4.0/

This article has been accepted for publication in IEEE Access. This is the author's version which has not been fully edited and content may change prior to final publication. Citation information: DOI 10.1109/ACCESS.2025.3565226

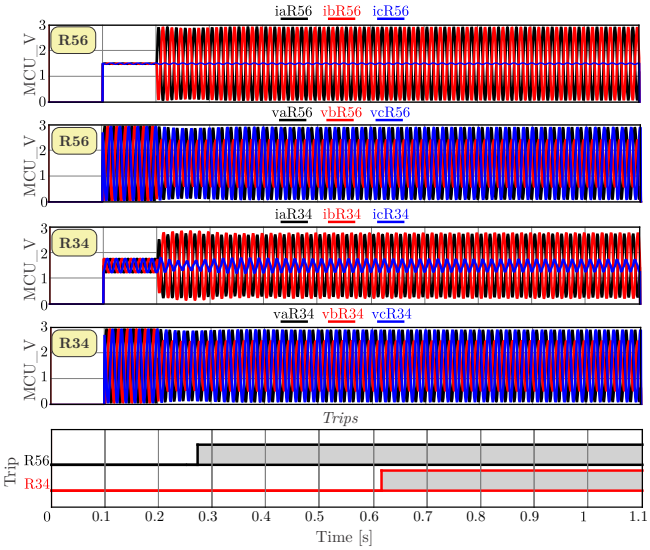

FIGURE 21. Real-time experiment V – 20 Ohm double-line fault in path 5–6 considering scenario 4 (grid-connected operating mode).

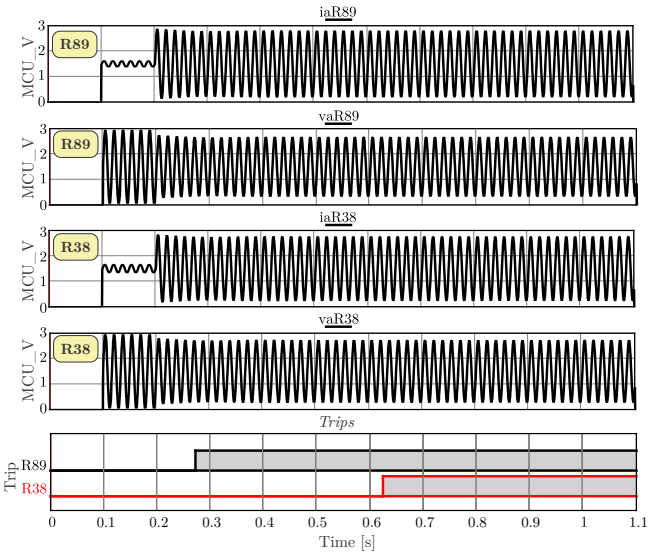

FIGURE 22. Real-time experiment VI – 20 Ohm single-line-to-ground fault in path 8–1 considering scenario 4 (grid-connected operating mode).

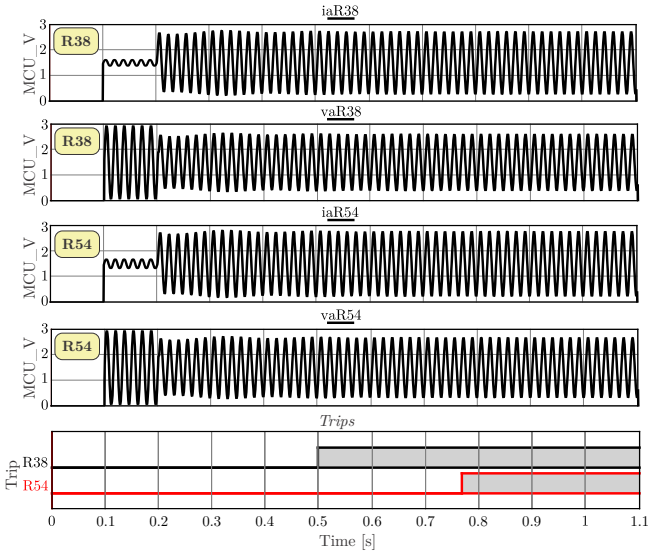

FIGURE 23. Real-time experiment VII – 15 Ohm single-line-to-ground fault in path 3–8 considering scenario 2 (grid-connected operating mode).

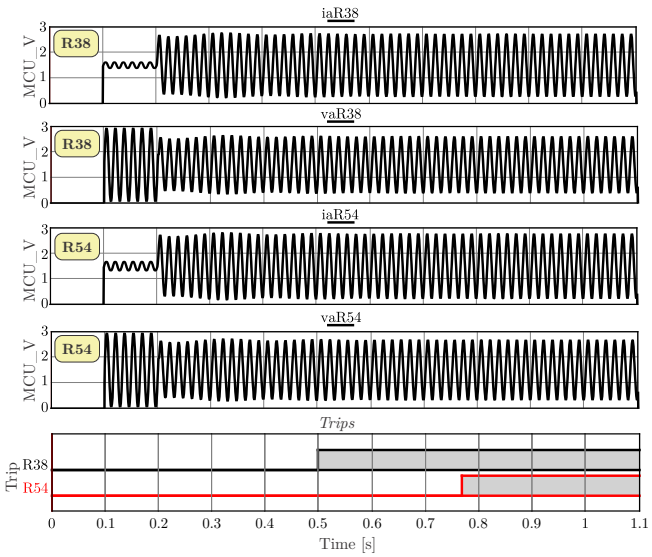

FIGURE 24. Real-time experiment VIII – 10 Ohm three-phase fault in path 5–8 considering scenario 6 (islanded operating mode with self-healing).

our method exhibited an average deviation of only 0.029 s (equivalent to 1.74 cycles at 60 Hz). This deviation falls well within the expected range for commercial relays, reinforcing the competitive performance in terms of response accuracy of the proposed protection.

VI. DISCUSSION

A key feature of an effective MG protection method is its ability to handle different configurations, scenarios, and fault behaviors. In a grid-connected mode, where fault currents are higher, the protection system must be dependable and well-coordinated. Conversely, in an islanded mode, where fault currents and voltages can be close to nominal values, the protection method should be both reliable and sensitive. The proposed hybrid tripping protection curve, presented in Section III-B, was carefully designed to address these challenges in MG protection considering both operating modes. Additionally, its simplicity allows for easy integration into low-cost hardware and seamless incorporation into the optimized protection coordination problem without significant concerns.

The validation of the proposed strategy through HIL testing on the TMSF28335 microcontroller with RTDS provided a reliable approximation to real-world conditions, enabling the evaluation of the protection method under distinct fault scenarios in MGs. Using a commercially available microcon-

This work is licensed under a Creative Commons Attribution 4.0 License. For more information, see https://creativecommons.org/licenses/by/4.0/

This article has been accepted for publication in IEEE Access. This is the author's version which has not been fully edited and content may change prior to final publication. Citation information: DOI 10.1109/ACCESS.2025.3565226

troller also indicated scalability, making the approach suitable for potential deployment in real-world applications. Furthermore, future validation in other testbeds and MG systems could strengthen the robustness of the method in different experimental setups. Thus, this work presented a practical framework for further refinement and potential application of the protection strategy in real MG environments by industry professionals and engineers.

VII. CONCLUSION

The proposed adaptive hybrid-tripping strategy achieved fast primary tripping (30–530.8 ms in 90% of all cases) while maintaining robust coordination (coordination time intervals ranging from 200 to 595.3 ms in 95% of all cases) for both grid-connected and islanded operating modes. The backup relays operated within 894.6 ms for 95% of the fault conditions considering both operating modes. Real-time validation with HIL tests demonstrated the feasibility and simplicity of embedding the proposed protection into low-cost MCUs. The experimental results closely aligned with the simulated outcomes, with maximum deviations below 64 ms. Thus, all simulations and experimental tests performed were able to confirm the dependability of the proposed protection considering the islanded and grid-connected operating conditions.

This paper did not cover certain aspects, such as variations in DG loading levels, fault inception angles, high impedance faults and the occurrence of concurrent faults in the MG. Moreover, evaluating the performance of different optimization algorithms was not the focus of this study. These limitations should be addressed in future studies.

ACKNOWLEDGMENT

The authors would like to thank the São Carlos School of Engineering, University of São Paulo, São Carlos, Brazil, for the facilities provided.

REFERENCES

[1] M. Green, "Community power," *Nat. Energy*, vol. 1, no. 3, p. 16014, 2016, doi: 10.1038/nenergy.2016.14.

[2] B. Chen, J. Wang, X. Lu, C. Chen, and S. Zhao, "Networked microgrids for grid resilience, robustness, and efficiency: A review," *IEEE Trans. Smart Grid*, vol. 12, no. 1, pp. 18–32, 2021, doi: 10.1109/TSG.2020.3010570.

[3] M. H. Saeed, F. Wang, B. A. Kalwar, and S. Iqbal, "A review on microgrids' challenges & perspectives," *IEEE Access*, vol. 9, pp. 166502–166517, 2021, doi: 10.1109/ACCESS.2021.3135083.

[4] C. Ceja-Espinosa, M. Pirnia, and C. A. Cañizares, "An affine arithmetic-based energy management system for cooperative multi-microgrid networks," *IEEE Trans. Smart Grid*, vol. 15, no. 2, pp. 1317–1329, 2024, doi: 10.1109/TSG.2023.3306702.

[5] A. Hirsch, Y. Parag, and J. Guerrero, "Microgrids: A review of technologies, key drivers, and outstanding issues," *Renew. Sustain. Energ. Rev.*, vol. 90, pp. 402–411, 2018, doi: 10.1016/j.rser.2018.03.040.

[6] I. Serban, S. Céspedes, C. Marinescu, C. A. Azurdia-Meza, J. S. Gómez, and D. Sáez, "Communication requirements in microgrids: A practical survey," *IEEE Access*, vol. 8, pp. 47694–47712, 2020, doi: 10.1109/ACCESS.2020.2977928.

[7] E. Espina, J. Llanos, C. Burgos-Mellado, R. Cárdenas-Dobson, M. Martínez-Gómez, and D. Sáez, "Distributed control strategies for microgrids: An overview," *IEEE Access*, vol. 8, pp. 193412–193448, 2020, doi: 10.1109/ACCESS.2020.3032378.

[8] S. Parhizi, H. Lotfi, A. Khodaei, and S. Bahramirad, "State of the art in research on microgrids: A review," *IEEE Access*, vol. 3, pp. 890–925, 2015, doi: 10.1109/ACCESS.2015.2443119.

[9] P. H. A. Barra, D. V. Coury, and R. A. S. Fernandes, "A survey on adaptive protection of microgrids and distribution systems with distributed generators," *Renew. Sustain. Energ. Rev.*, vol. 118, p. 109524, 2020, doi: 10.1016/j.rser.2019.109524.

[10] M. W. Altaf, M. T. Arif, S. N. Islam, and M. E. Haque, "Microgrid protection challenges and mitigation approaches–a comprehensive review," *IEEE Access*, vol. 10, pp. 38895–38922, 2022, doi: 10.1109/ACCESS.2022.3165011.

[11] J. Reilly and S. S. M. Venkata, "Microgrid protection: Its complexities and requirements [Guest Editorial]," *IEEE Power Energy Mag.*, vol. 19, no. 3, pp. 14–19, 2021, doi: 10.1109/MPE.2021.3057949.

[12] L. He, Z. Shuai, X. Chu, W. Huang, Y. Feng, and Z. J. Shen, "Waveform Difference Feature-Based Protection Scheme for Islanded Microgrids," *IEEE Trans. Smart Grid*, vol. 12, no. 3, pp. 1939–1952, 2021, doi: 10.1109/TSG.2020.3048191.

[13] H. Beder, B. Mohandes, M. S. E. Moursi, E. A. Badran, and M. M. E. Saadawi, "A new communication-free dual setting protection coordination of microgrid," *IEEE Trans. Power Del.*, vol. 36, no. 4, pp. 2446–2458, 2021, doi: 10.1109/TPWRD.2020.3041753.

[14] A. A. Aboelnaga and M. A. Azzouz, "Adaptive current-angle-based phase selection for microgrids with inverter-interfaced renewable energy sources," *IEEE Trans. Smart Grid*, pp. 1–12, 2021, doi: 10.1109/TSG.2021.3112664.

[15] M. G. M. Zanjani, K. Mazlumi, and I. Kamwa, "Application of μPMUs for adaptive protection of overcurrent relays in microgrids," *IET Gener. Transm. Distrib.*, vol. 12, no. 18, pp. 4061–4068, 2018, doi: 10.1049/iet-gtd.2018.5898.

[16] N. K. Sharma and S. R. Samantaray, "PMU assisted integrated impedance angle-based microgrid protection scheme," *IEEE Trans. Power Del.*, vol. 35, no. 1, pp. 183–193, 2020, doi: 10.1109/TPWRD.2019.2925887.

[17] K. Saleh, M. A. Allam, and A. Mehrizi-Sani, "Protection of inverter-based islanded microgrids via synthetic harmonic current pattern injection," *IEEE Trans. Power Del.*, vol. 36, no. 4, pp. 2434–2445, 2021, doi: 10.1109/TPWRD.2020.2994558.

[18] W. T. El-Sayed, M. A. Azzouz, H. H. Zeineldin, and E. F. El-Saadany, "A harmonic time-current-voltage directional relay for optimal protection coordination of inverter-based islanded microgrids," *IEEE Trans. Smart Grid*, vol. 12, no. 3, pp. 1904–1917, 2021, doi: 10.1109/TSG.2020.3044350.

[19] W. T. El-Sayed, E. F. El-Saadany, and H. H. Zeineldin, "Interharmonic differential relay with a soft current limiter for the protection of inverter-based islanded microgrids," *IEEE Trans. Power Del.*, vol. 36, no. 3, pp. 1349–1359, 2021, doi: 10.1109/TPWRD.2020.3006791.

[20] E. Dehghanpour, M. Normandeau, G. Joós, and Y. Brissette, "A protection system for inverter interfaced microgrids," *IEEE Trans. Power Del.*, vol. 37, no. 3, pp. 2314–2325, 2022, doi: 10.1109/TPWRD.2021.3110199.

[21] P. Gadde and S. M. Brahma, "Topology-agnostic, scalable, self-healing, and cost-aware protection of microgrids," *IEEE Trans. Power Del.*, vol. 37, no. 4, pp. 3391–3400, 2022, doi: 10.1109/TPWRD.2021.3128880.

[22] J. Y. R. Wong, C. Tan, A. H. A. Bakar, and H. S. Che, "Selectivity problem in adaptive overcurrent protection for microgrid with inverter-based distributed generators (IBDG): Theoretical investigation and HIL verification," *IEEE Trans. Power Del.*, vol. 37, no. 4, pp. 3313–3324, 2022, doi: 10.1109/TPWRD.2021.3126897.

[23] J. E. Santos-Ramos, S. D. Saldarriaga-Zuluaga, J. M. López-Lezama, N. Muñoz-Galeano and W. M. Villa-Acevedo, "Microgrid Protection Coordination Considering Clustering and Metaheuristic Optimization," *Energies*, vol. 17, no. 1, 2024, doi: doi.org/10.3390/en17010210.

[24] M. Vygoder, F. Banihashemi, J. Gudex, A. Eggebeen, G. Oriti and R. M. Cuzner, "A Novel Protection Design Process to Increase Microgrid Resilience," *IEEE Transactions on Industry Applications*, vol. 60, no. 7, 2024, doi: 10.1109/TIA.2024.3377171

[25] S. P. Tiwari, "An efficient protection scheme for critical fault detection in microgrid under uncertain scenarios using deep learning algorithm," *Electrical Engineering*, 2024, doi: 10.1007/s00202-024-02861-3

[26] A. Najar, H. K. Karegar and S. Esmaeilbeigi, "Multi-agent protection scheme for microgrid using deep learning," *IET Renewable Power Generation*, vol. 18, p. 663-678, 2024, doi: 10.1049/rpg2.12929

[27] R. Kumari and B. K. Naick, "Enhancing protection in AC microgrids: An adaptive approach with ANN and ANFIS models," *Com-*

This work is licensed under a Creative Commons Attribution 4.0 License. For more information, see https://creativecommons.org/licenses/by/4.0/

This article has been accepted for publication in IEEE Access. This is the author's version which has not been fully edited and content may change prior to final publication. Citation information: DOI 10.1109/ACCESS.2025.3565226

puters and Electrical Engineering, vol. 115, p. 109103,, 2024, doi: 10.1016/j.compeleceng.2024.109103

[28] A. F. Qusayer and S. M. S. Hussain, "Communication Assisted Protection Scheme Based on Artificial Neural Networks for Multi-Microgrid," *IEEE Access*, vol. 12, p. 24442-24452, 2024, doi: 10.1109/ACCESS.2024.3352027

[29] IEEE, "IEEE standard for inverse-time characteristics equations for overcurrent relays," *IEEE Std C37.112-2018 (Revision of IEEE Std C37.112-1996)*, pp. 1–25, 2019, doi: 10.1109/IEEESTD.2019.8635630.

[30] N. El-Naily, S. M. Saad, T. Hussein, and F. A. Mohamed, "A novel constraint and non-standard characteristics for optimal over-current relays coordination to enhance microgrid protection scheme," *IET Gener. Transm. Distrib.*, vol. 13, no. 6, pp. 780–793, 2019, doi: 10.1049/iet-gtd.2018.502.

[31] A. Darabi, M. Bagheri, and G. B. Gharehpetian, "Highly sensitive microgrid protection using overcurrent relays with a novel relay characteristic," *IET Renew. Power Gener.*, vol. 14, no. 7, pp. 1201–1209, 2020, doi: 10.1049/iet-rpg.2019.0793.

[32] S. D. Saldarriaga-Zuluaga, J. M. López-Lezama, and N. Muñoz-Galeano, "Optimal coordination of overcurrent relays in microgrids considering a non-standard characteristic," *Energies*, vol. 13, no. 4, p. 922, 2020, doi: 10.3390/en13040922.

[33] S. Chakraborty and S. Das, "Communication-less protection scheme for AC microgrids using hybrid tripping characteristic," *Electr. Power Syst. Res.*, vol. 187, p. 106453, 2020, doi: 10.1016/j.epsr.2020.106453.

[34] H. C. Kiliçkiran, İ. Şengör, H. Akdemir, B. Kekezoğlu, O. Erdinç, and N. G. Paterakis, "Power system protection with digital overcurrent relays: A review of non-standard characteristics," *Electr. Power Syst. Res.*, vol. 164, pp. 89–102, 2018, doi: 10.1016/j.epsr.2018.07.008.

[35] K. A. Saleh, H. H. Zeineldin, A. Al-Hinai, and E. F. El-Saadany, "Optimal coordination of directional overcurrent relays using a new time–current–voltage characteristic," *IEEE Trans. Power Del.*, vol. 30, no. 2, pp. 537–544, 2015, doi: 10.1109/TPWRD.2014.2341666.

[36] R. Bekhradian, M. Davarpanah, and M. Sanaye-Pasand, "Novel approach for secure islanding detection in synchronous generator based microgrids," *IEEE Trans. Power Del.*, vol. 34, no. 2, pp. 457–466, 2019, doi: 10.1109/TPWRD.2018.2869300.

[37] R. Sepehrzad, A. Mahmoodi, S. Y. Ghalebi, A. R. Moridi, and A. R. Seifi, "Intelligent hierarchical energy and power management to control the voltage and frequency of micro-grids based on power uncertainties and communication latency," *Electr. Power Syst. Res.*, vol. 202, p. 107567, 2022, doi: 10.1016/j.epsr.2021.107567.

[38] Z. Wang, L. Mu and C. Fang, "Renewable Microgrid Protection Strategy Coordinating with Current-based Fault Control," *Journal of Modern Power Systems and Clean Energy*, vol. 10, p. 1679-1689, 2022, doi: 10.35833/MPCE.2022.000079.

[39] IEEE, "IEEE standard for interconnection and interoperability of distributed energy resources with associated electric power systems interfaces," *IEEE Std 1547-2018 (Revision of IEEE Std 1547-2003)*, 2018, doi: 10.1109/IEEESTD.2018.8332112.

[40] IEEE, "IEEE Recommended Practice for Protection and Coordination of Industrial and Commercial Power Systems (IEEE Buff Book)," *IEEE Std 242-2001 (Revision of IEEE Std 242-1986*, 2001, doi: 10.1109/IEEESTD.2001.93369.

[41] IEEE, "IEEE guide for power system protective relay applications over digital communication channels," *IEEE Std C37.236-2013*, 2013, doi: 10.1109/IEEESTD.2013.6504869.

[42] M. Agustoni, P. Castello, and G. Frigo, "Phasor measurement unit with digital inputs: Synchronization and interoperability issues," *IEEE Trans. Instrum. Meas.*, vol. 71, pp. 1–10, 2022, doi: 10.1109/TIM.2022.3176800.

[43] V. Couto and M. Moreto, "High Impedance Fault Detection on Microgrids Considering the Impact of VSC Based Generation," *IEEE Access*, vol. 11, pp. 89550-89560, 2023, doi: 10.1109/ACCESS.2023.3305958.

[44] CIGRE Working Group C6-04, "Benchmark systems for network integration of renewable and distributed energy resources," *Technical Brochure 575*, 2014.

[45] Schweitzer Engineering Laboratories, "SEL-751 Feeder Protection Relay," Available in: https://selinc.com/api/download/10734/

[46] Texas Instruments, "Users Guide – LAUNCHXL-F28379D Overview," Available in: https://www.ti.com/lit/ug/sprui77c/sprui77c.pdf?ts=1740649637514&ref_url=https%253A%252F%252F

PEDRO HENRIQUE AQUINO BARRA received his B.Sc. and M.Sc. degrees in Electrical Engineering from the Federal University of Uberlândia, Brazil, in 2015 and 2017, respectively. In 2022, he earned his Ph.D. degree in Electrical Engineering from the University of São Paulo, São Carlos, Brazil. He is currently an Adjunct Professor at the Federal University of Uberlândia, Brazil. His research interests include power system protection, microgrids, distribution systems, and smart grids.

RICARDO AUGUSTO SOUZA FERNANDES (Senior Member, IEEE) received his B.Sc. degree in Electrical Engineering from the Educational Foundation of Barretos, Barretos, in 2006, and his M.Sc. and Ph.D. degrees in Electrical Engineering from the University of São Paulo, São Carlos, Brazil, in 2009 and 2011, respectively. In 2015 and 2017, he was a Visiting Professor at the Polytechnic Institute of Porto. He is currently an Assistant Professor at the University of São Paulo, São Carlos, Brazil. His research interests include embedded systems, signal processing, machine learning, and smart grids.

DENIS VINICIUS COURY received his B.Sc. degree in Electrical Engineering from the Federal University of Uberlândia, Brazil, in 1983, his M.Sc. degree from the São Carlos School of Engineering-University of São Paulo, Brazil, in 1986, and his Ph.D. degree from Bath University, U.K., in 1992. He worked at the Technological Research Institute (IPT), São Paulo, Brazil, from 1985 to 1986. He joined the Department of Electrical and Computer Engineering, University of São Paulo, São Carlos, Brazil, in 1986, where he is currently a Full Professor in the Power Systems Group. He spent his Sabbatical at Cornell University (USA) from 1999 to 2000. His research interests include power system protection, expert systems, smart grids and microgrids.

This work is licensed under a Creative Commons Attribution 4.0 License. For more information, see https://creativecommons.org/licenses/by/4.0/